SECTION 5 OF CHAMPLAIN BRIDGE

2D NON-LINEAR ANALYSES OF P7 IN SPAN 28W-29W

REPORT SUBMITTED TO:

Ponts Jacques Cartier et Champlain Inc.

Contract Number: 62076

Denis Mitchell, ing., Ph.D.

Denis Mitchell Consulting Inc.

May 25, 2015

Contents

1. Introduction

The objective of this study was to gain a better understanding of the performance of a typical edge girder in a typical span of Section 5 of the Champlain Bridge. This study involves two different phases:

- Develop a 2-D non-linear finite element model of a precast post-tensioned girder of the Champlain Bridge as originally constructed.
- Carry out analyses to study various scenarios to gain a better understanding of the performance of a typical girder under different conditions.

The computer program VecTor2 was used to carry out the study. This analysis package can account for the non-linear stress-strain relationships of the concrete, reinforcing steel and prestressing tendons. Because of the features of this program, various behavioural aspects such as concrete cracking, flexural yielding, concrete crushing and shear distress can be determined. In addition, the program enables an assessment of long-term effects, including concrete shrinkage as well the effects of creep on the concrete stress-strain relationship.

The following scenarios were investigated:

- Loss of post-tensioning reinforcement due to corrosion in midspan region to study this effect and also to simulate the critical crack that resulted in the urgent need for the installation of the super beam
- Loss of inclined tendon(s) to simulate corrosion where reflective cracking has occurred over the tendon
- The influence of external longitudinal post-tensioning (PTE).
- The influence of Queen Post 1 (QP1)
- The influence of Queen Post 2 (QP2)

A separate 3D linear elastic study was carried out by others (Massicotte, 2015) to determine the sharing of the loads among the seven girders in a typical span for both dead loads and different truck loading cases as well as for different strengthening methods. This 3D analysis enabled the determination of forces to be applied to the 2D finite element model of a typical edge girder.

The study concentrated on the behavior of edge girder P7 in span 28W-29W in Section 5 of the Champlain Bridge for a degree of corrosion that simulated the observations and assessment made in 2014. In addition to the finite element analysis an additional assessment was made using sectional analysis to study the effects of the degree of corrosion on the predicted crack widths at midspan.

2. Material Properties

2.1 Concrete

Figure 2.1 shows the concrete compressive strengths obtained from 94 core samples taken from girders in Section 5. This data on the strength of the cores was obtained from a report by TECHNISOL INC. (2006).
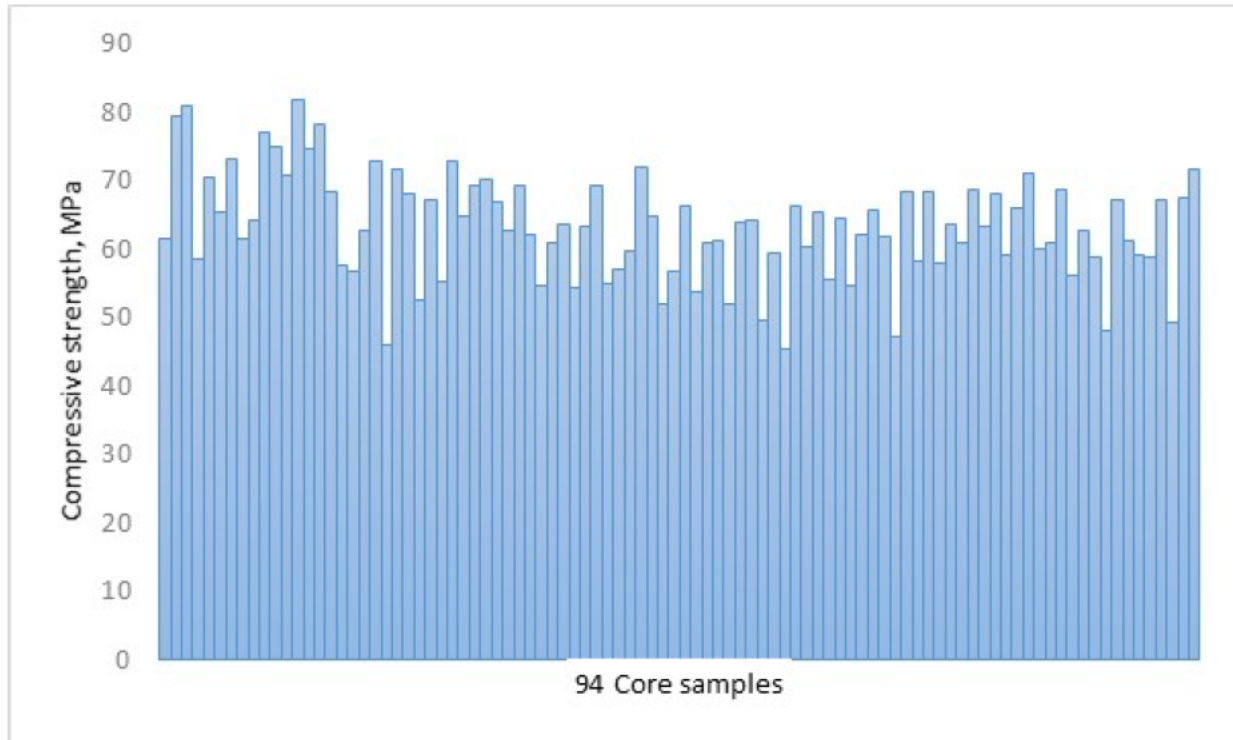
Fig. 2.1: Concrete compressive strengths obtained from core samples in Section 5 of bridge.

The compressive strengths vary from 45.5 to 81.7 MPa. The average compressive strength is 63.2 MPa. The equivalent specified compressive strength, f_c', used for evaluation was determined using the procedure given in Clause A14.1.2 of CSA S6-06. The equivalent specified compressive strength, f_c', was determined to be 53.9 MPa for the evaluation of Girder P7 in span 28W-29W. For all of the analyses a concrete tensile strength of $0.33\sqrt{f_c'} = 2.42$ MPa was assumed.

For short-term loading the concrete was modelled with a non-linear stress-strain relationship with a peak compressive strain of 0.0023 for sectional analysis and 0.0022 for the non-linear finite element analysis.

For the long-term concrete stress-strain relationship the creep factor was determined using the creep equations given in CSA S6-06, resulting in a creep factor of 2.2 at an age of 51 years. The

non-linear stress-strain relationship was adjusted so that the peak compressive strain was 0.00704.

2.2 Reinforcing Steel and Prestressing Wires

Girder P7 contains 24 post-tensioned tendons. Each tendon consists of 12 – 7 mm (0.276 in.) diameter prestressing wires. The area of one tendon containing 12 wires was taken as 462 mm^2. Clause 14.7.4.4 of CSA S6-06 recommends a value of 1600 MPa for the ultimate strength of the prestressing steel, f_{pu}, to be used for the evaluation of bridges constructed before 1963. However, the original calculations (Warycha and Skotecky) for the design of Section 5 indicate that the ultimate strength, f_{pu}, of the prestressing wires was 228 ksi (1572 MPa) for the design of the girders.

The more conservative value for f_{pu} of 1572 MPa was used in the 2D non-linear model and in the sectional analysis.

The original calculations (Warycha and Skotecky) for the design of Section 5 indicate that they had used an allowable stress in the reinforcing steel of 20,100 psi, indicating that the yield stress was likely 40,000 psi (275 MPa). This yield stress is consistent with the typical reinforcement used during the period of construction and is within the range of yield strengths recommended by CSA S6-06 for evaluation.

It was assumed that the yield strength of the normal reinforcing bars was 275 MPa.

The short-term modulus of elasticity for the prestressing tendons and reinforcing steel was taken as 200,000 MPa.

The long-term modulus of the prestressing steel was determined using the loss calculations given in CSA S6-06, resulting in a reduced modulus of 171,800 MPa at an age of 51 years.

3. Estimation of Degree of Corrosion of Tendons in Girder P7 in 2014

Observations on site indicated that severe corrosion was taking place mainly in the midspan regions, at the level of the bottom tendons, in Girder P7 of span 28W-29W. Figure 3.1 gives the data on the extent of corrosion, concluded by the consultants, based on observations on site at midspan of girder P7.

Tendon Numbers	Estimated loss due to corrosion	
3, 6, 11, 12, 13, 21, 22, 23, 24	100%	
15, 16, 17, 18	50%	
7	25%	
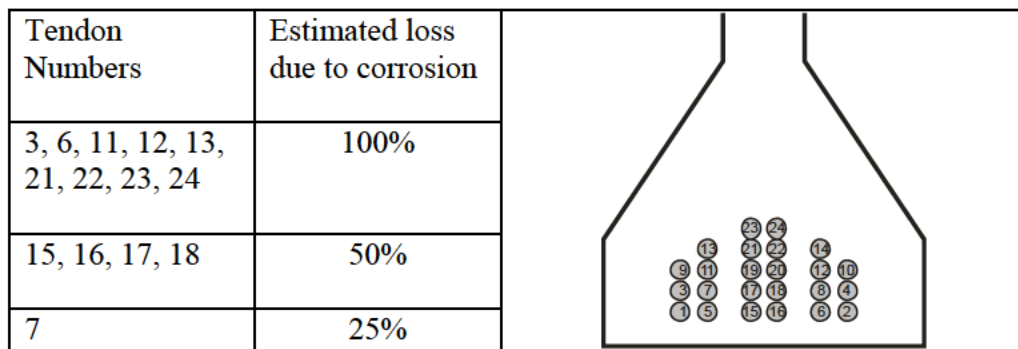
Fig. 3.1: Assumed Degree of corrosion at midspan (December 2014)

Observations on site and access holes in the web of P7 indicate that the corrosion of the tendons outside of the midspan region had somewhat less corrosion than the tendons in the midspan region. This inspection also revealed that there was some corrosion of the stirrups.

This information provided some guidance on the degree of corrosion in P7 before it suffered major distress.

4. Loads, Load Factors and Material Resistance factors

4.1 Loads and Load Factors

The dead load was determined and checked with the analysis obtained from CSI Bridge (3D study).

The live loading due to trucks and vehicular traffic conformed to the requirements of S6-06 for CL-625 truck loading and specified lane loadings. For example, for maximum moment in girder P7 at midspan the following cases were studied:

- CL-625 loading on the exterior southbound lane
- CL-625 loading on two lanes (exterior and adjacent southbound lanes)
- CL-625 loading on all three southbound lanes
- CL-625 lane loading on the exterior southbound lane
- CL-625 lane loading on two lanes (exterior and adjacent southbound lanes)
- CL-625 lane loading on all three southbound lanes

For these cases the trucks were positioned to cause maximum moment near midspan.

A value of 0.25 was assumed for the dynamic load allowance for cases with the CL-625 loading (first 3 cases listed above). Modification factors for multi-lane loading were 1.0, 0.9 and 0.8 for one lane, 2 lanes and 3 lanes loaded, respectively. From the 3D structural analysis it was determined that the most critical case for maximum moment at midspan was for the CL-625 lane loading on all three southbound lanes.

The following load factors were obtained from Section 14 – "Evaluation" of CSA S6-06, considering the estimated target reliability indices and the type of loading:

- Dead load factor for girders: 1.09 (category D1)
- Dead load factor for diaphragms, deck, asphalt and barriers: 1.18 (category D2)
- Live load factor: 1.63 (truck loading)

4.2 Material Resistance Factors

The material resistance factors used to determine the factored resistances of girder P7 conformed to the requirements in Section 8.4.6 of CSA S6-06. These material resistance factors are as follows:

- Material resistance factor for concrete, ϕ_c 0.75
- Material resistance factor for reinforcing bars, ϕ_s 0.90
- Material resistance factor for prestressing steel, ϕ_p 0.95

5. Sectional Analysis for Flexural Behaviour at Midspan without Strengthening Measures

5.1 Midspan Moments

The following moments at midspan in girder P7 were determined from analyses:

- Dead loads D1   10,069 kNm
- Dead load, D2   4,360 kNm
- Maximum live loading   6,098 kNm

These loads result in a maximum service load moment, $M_{service}$, at midspan of 20,526 kNm.

Using the load factors given in Section 3.1, the resulting maximum factored moment, M_f, at midspan is 26,059 kNm.

5.2 Cross-Sectional Details and Material Modelling

A sectional analysis was carried out using the program Response 2000 (Bentz 2015). The cross-sectional details and material properties for the short-term flexural predictions are given in Fig. 5.1. The concrete compressive strength corresponds to the 51-year old concrete strength determined in accordance with CSA S6-06 (see Section 2).

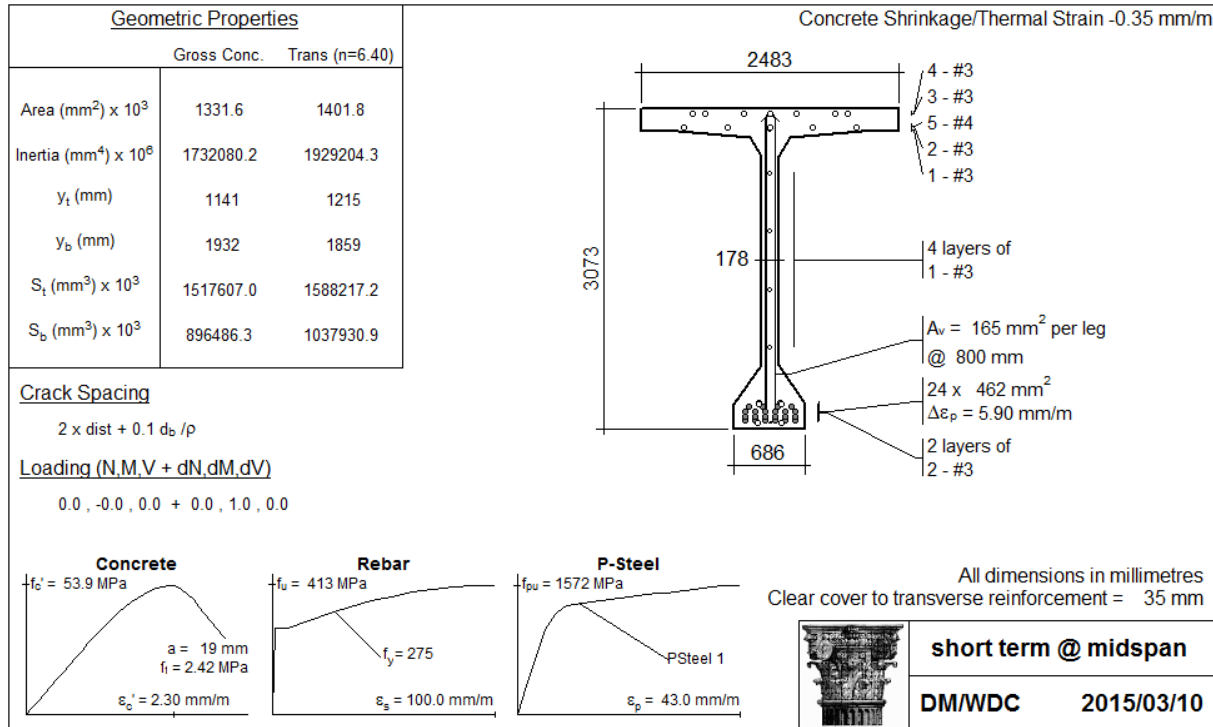Fig. 5.1: Input for Response 2000 at midspan section for short-term predictions

Figure 5.2 shows the changes to the material properties to account for long-term effects at an age of 51 years. The concrete compressive stress-strain relationship has been adjusted to account for creep effects and the modulus of elasticity of the prestressing tendons has been reduced to account for relaxation losses (see Section 2).
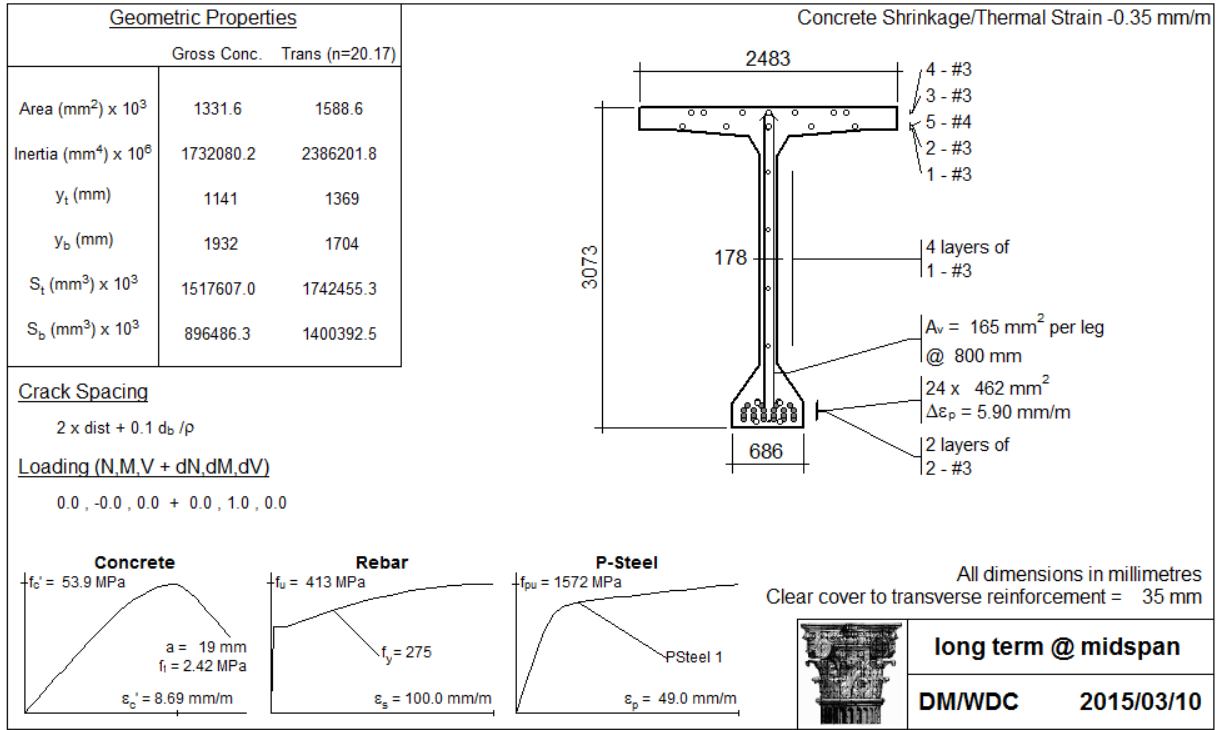
Fig. 5.2: Input for Response 2000 at midspan section for long-term predictions

5.3 Modelling Effects of Tendon Loss Due to Corrosion

Figure 5.3 shows the layout of the original 24 post-tensioned tendons at midspan. Table 5.1 gives the order of tendon removal in the analytical model to simulate the loss of tendons at midspan due to corrosion. For this simulation of corrosion, a pair of tendons was removed from each layer starting from the bottommost layer as shown in Table 5.1.
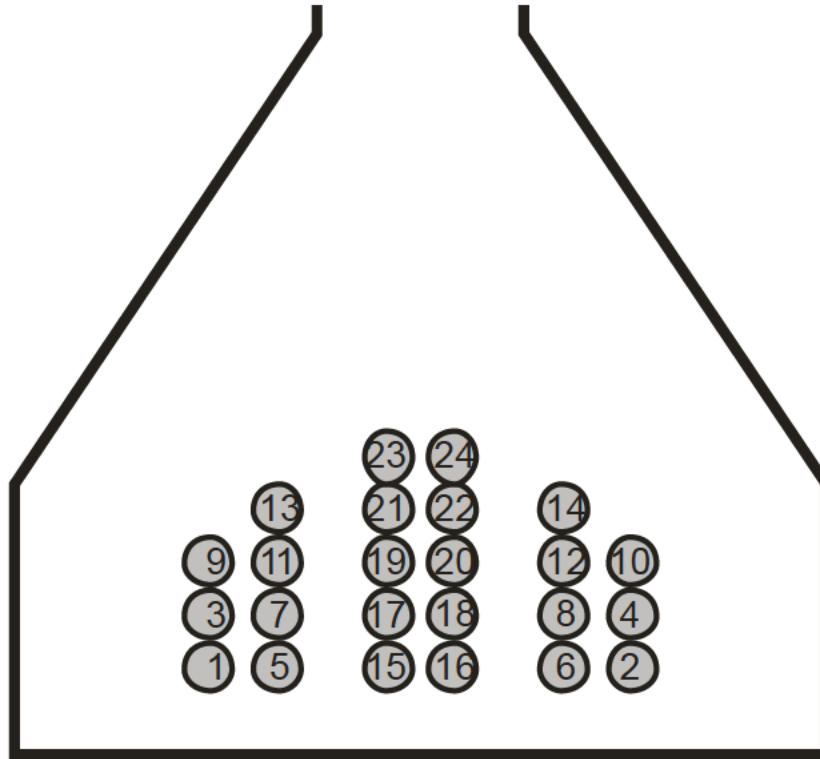
Fig. 5.3: Tendon layout

Table 5.1: Order of tendon removal to simulate losses due to corrosion

# tendons remaining	# tendons lost	Tendons removed
24	0	-
22	2	15, 16
20	4	15, 16, 17, 18
18	6	15, 16, 17,18, 19, 20
16	8	15, 16, 17,18, 19, 20, 21,22
14	10	15, 16, 17,18, 19, 20, 21, 22, 23,24
12	12	15, 16, 17,18, 19, 20, 21, 22, 23,24,1, 2
10	14	15, 16, 17,18, 19, 20, 21, 22, 23,24,1, 2, 5, 6
8	16	15, 16, 17,18, 19, 20, 21, 22, 23,24,1, 2, 5, 6, 3, 4
6	18	15, 16, 17,18, 19, 20, 21, 22, 23,24,1, 2, 5, 6, 3, 4, 7, 8

5.4 Influence of Tendon Losses on Flexural Strength at Midspan

Fig. 5.4 shows the predicted factored moment, M_r, at midspan as the number of prestressing tendons is reduced to simulate varying degrees of corrosion. For these predictions, the short-term

properties were used (see Fig. 5.1) and concrete shrinkage was neglected. This figure also shows the required factored moment, M_f, and the service load moment, $M_{service}$, at midspan.

As can be seen from Fig. 5.4 the factored flexural resistance at midspan is significantly greater than the required factored moment, for the case with no corrosion. When 10 tendons are lost due to corrosion the factored flexural resistance at midspan equals the required factored moment. The loss of 10 tendons due to corrosion corresponds to 41.7% of the 24 original tendons. When 13 tendons are lost due to corrosion (that is, 54% of the original tendons) it is predicted that the factored moment resistance would be equal to the service load moment.

It is noted that the ability of the 7 in. thick reinforced concrete web to develop horizontal shear resistance may limit the ability to develop the full moment capacity. This limit is shown in Fig. 5.4 for the case of the web without horizontal cracking. The influence of the horizontal cracking observed in some of the girders needs to be further investigated.
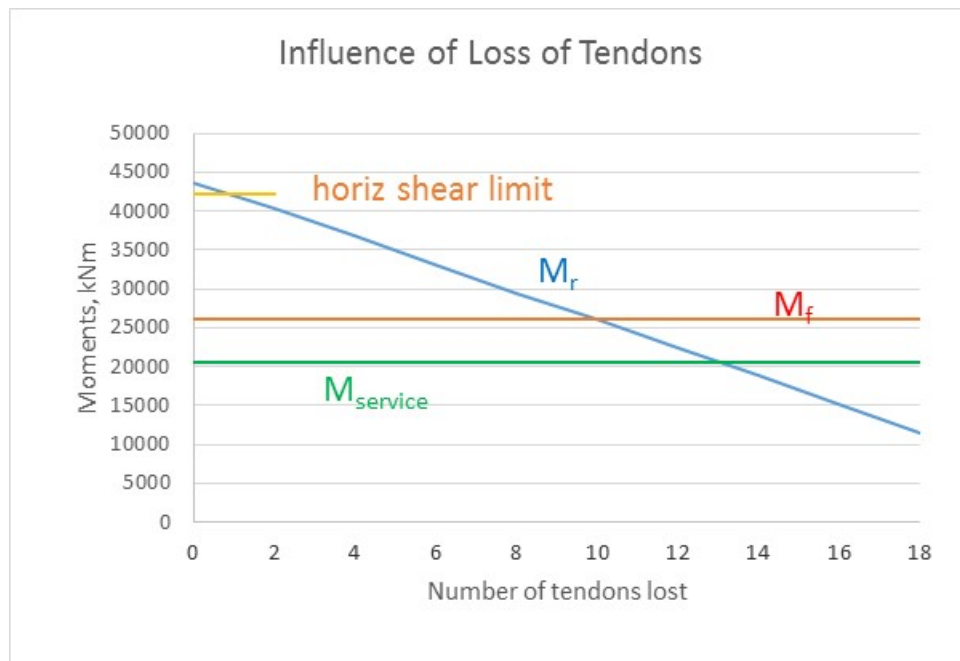
Fig. 5.4: Effect of loss of tendons on the factored moment resistance at midspan.

5.5 Predicted Crack Widths at Midspan under Service Loading

Figures 5.5 and 5.6 show the predicted crack widths at midspan as a function of the number of tendons that are lost due to corrosion for the case of full service loading (D+L). The predicted cracking at the bottom of the flange is given in Fig. 5.5 and the maximum predicted cracking in the web is given in Fig. 5.6.

The figures show the predictions for short-term loading and long-term loading. The dead loads are due to long-term loading (51 years) while the live loading due to traffic is a

short-term, but repetitive loading. The expected crack width would likely lie between these two predictions, but would likely be closer to the long-term predictions due to the fact that about 70% of the midspan moment is due to sustained dead load.

It is noted that some of the concrete in the bottom flange had been replaced and therefore the predictions for the crack widths in the bottom flange are not expected to agree with the observed crack widths. Furthermore, girder P7 of span 28W-29W was strengthened with eternal horizontal post-tensioning in 1998. These effects are not included in this analysis but will be discussed later.

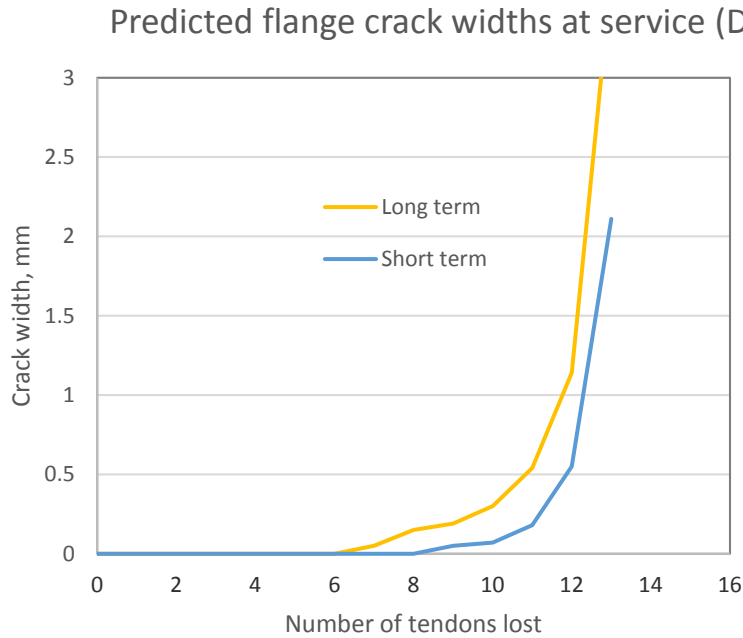**Predicted flange crack widths at service (D+L)**

Fig. 5.5: Predicted crack widths in flange at midspan due to D + L, as a function of the number of tendons lost due to corrosion.
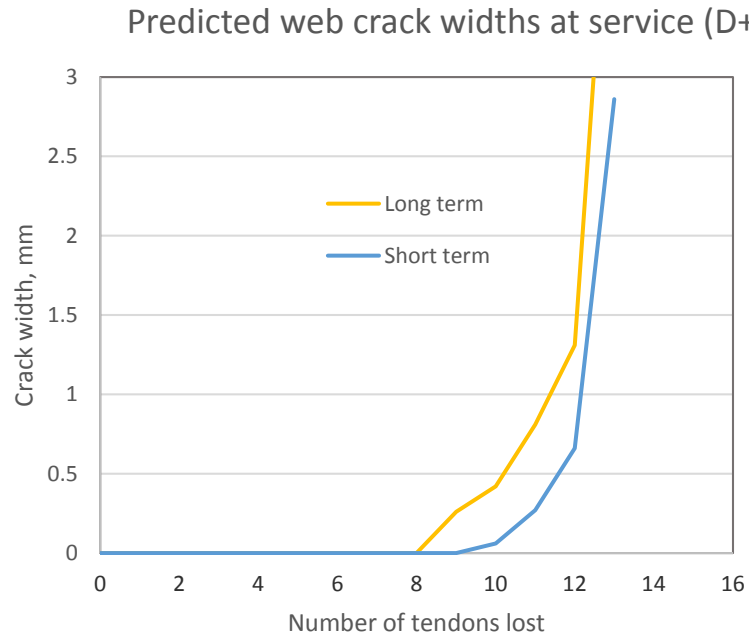
Fig. 5.6: Predicted maximum crack widths in web at midspan due to D + L, as a function of the number of tendons lost due to corrosion.

6. 2D Non-Linear Finite Element Model

6.1 Description of Finite Element Model

The finite element modelling was carried out with the program "VecTor2" (Vecchio 2015), version 3.8.

Fig. 6.1 shows the finite element mesh used to model the exterior girder, P7. The model includes the precast girder, one-half of the slab and one-half of the diaphragms between girders. The total length of the beam is 176 feet (53.64 m) and the distance between the centres of the bearings is 172 feet (52.42 m). The different coloured rectangular elements represent different concrete thicknesses and amounts of horizontal and vertical reinforcement. The post-tensioning tendons are also shown. The light blue elements represent groupings of 3 tendons while the dark blue elements are single tendons (12-7 mm diameter wires per tendon). There are 24 tendons in the girder.
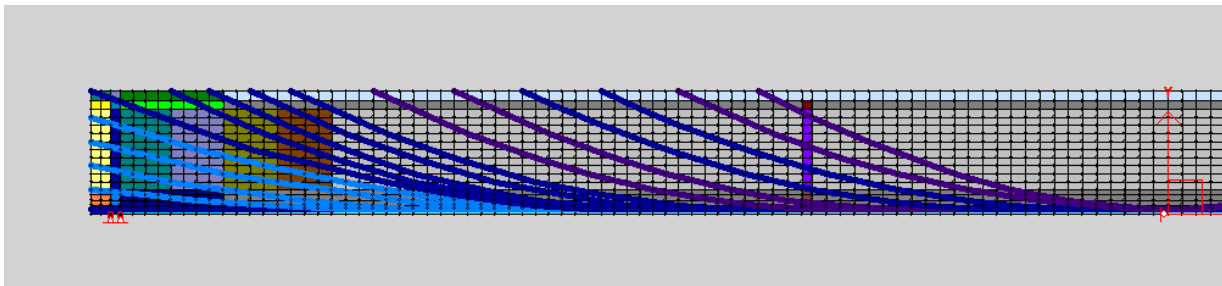

Fig. 6.1: Finite element model for P7 (symmetrical about midspan)

6.2 Determining Forces Applied to Girder P7

The 3D linear elastic model of span 28W-29W enabled the determination of forces in the super structure. This analysis was carried out using CSI Bridge. This analysis was used to determine the forces applied to girder P7 due to different live loading cases. These forces were applied to the 2D non-linear finite element model to be able to study the performance of girder P7 for different conditions.

The 2D non-linear analyses performed did not consider the redistribution of forces between girder P7 and the rest of the superstructure that may occur due to inelastic behavior of girder P7.

6.3 Accounting for Loss of Tendons and Stirrups due to Corrosion

In order to study the behaviour of girder P7 in span 28W-29W with the effects of corrosion, assumptions had to be made concerning the degree of corrosion of the tendons as well as the

stirrups. From the conclusions made by the consultants, based on observations on site (see Section 3), it was assumed that 11.25 tendons were lost at midspan due to corrosion leaving 12.75 tendons. This represents a loss of 46.9% of the tendons at midspan. A uniform degree of corrosion of 40% of the tendons was assumed for the tendons outside of the midspan region. In addition a uniform degree of corrosion of 40% of the stirrups was assumed.

Figure 6.2 shows the modelling of the loss of tendons due to corrosion, with the tendons in the midspan region (orange colour) indicating the concentrated corrosion assumed at midspan. In addition the cross-sectional areas of the stirrup reinforcement were reduced by 40%.
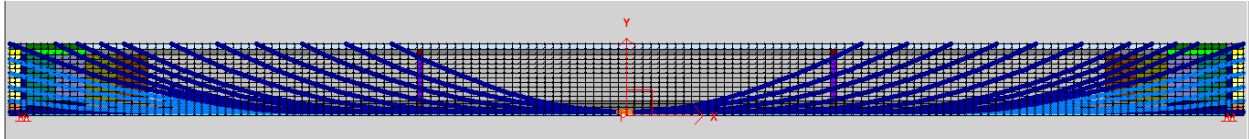
(a) Overall view
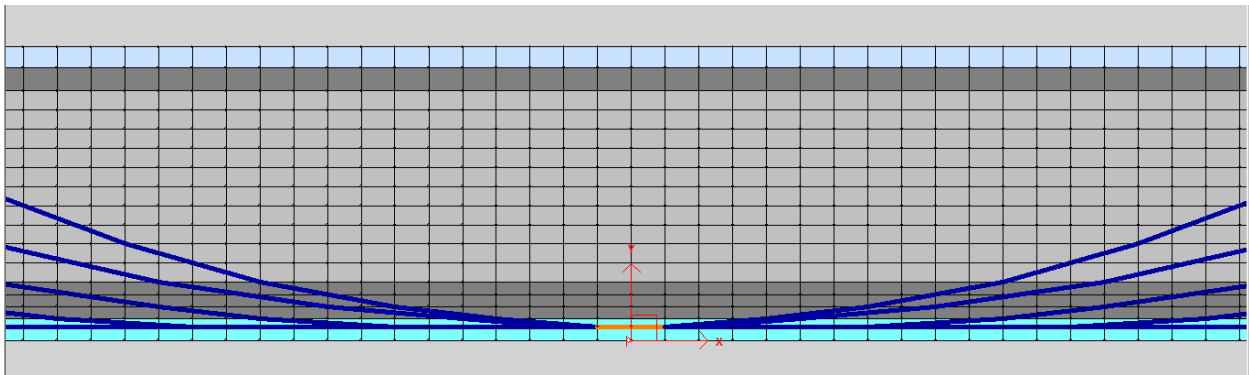
(a) Close-up of midspan region

Fig. 6.2: Modelling of corroded tendons

6.4 Accounting for Strengthening Measures

The effects of different strengthening measures, including external horizontal post-tensioning (PTE), Queen Post 1 (QP1) and Queen Post 2 (QP2), were first analysed using the 3D model. The forces acting on P7 from the 3D model were then applied to the 2D non-linear model to simulate the effects of strengthening.

The effects of the strengthening have been simulated in the 2D non-linear model by the application of loads on P7 to correspond to the linear elastic forces obtained from the 3D analysis of the entire bridge span with seven girders. Because the effects of the strengthening measures were modelled using applied forces, the stiffness of the added post-tensioning was neglected.

7. Predicted Behaviour for Live Loading Causing Maximum Moment at Midspan, Without Strengthening Measures

7.1 Loads Applied to the Finite Element Model for Maximum Moment at Midspan

The dead load was applied in two different load cases: one with just the girder self-weight (D1) and the other with the additional dead loads (D2), considering the slab, diaphragms, barrier, asphalt and an allowance for utilities, acting on the exterior girder. The midspan moment due to service dead loading is 14,430 kNm.

Figure 7.1 shows the shear force diagram that matches the shears from the 3-D model on the edge girder due to the critical live loading case for maximum moment at midspan. This controlling load case has 3 traffic lanes loaded with lane loads. The lane load consists of 80% of the CL-625 truck plus a uniformly distributed load of █ kN/m. Due to the fact that 3 lanes are loaded a modification factor for multiple lane loading equal to 0.80 was applied.
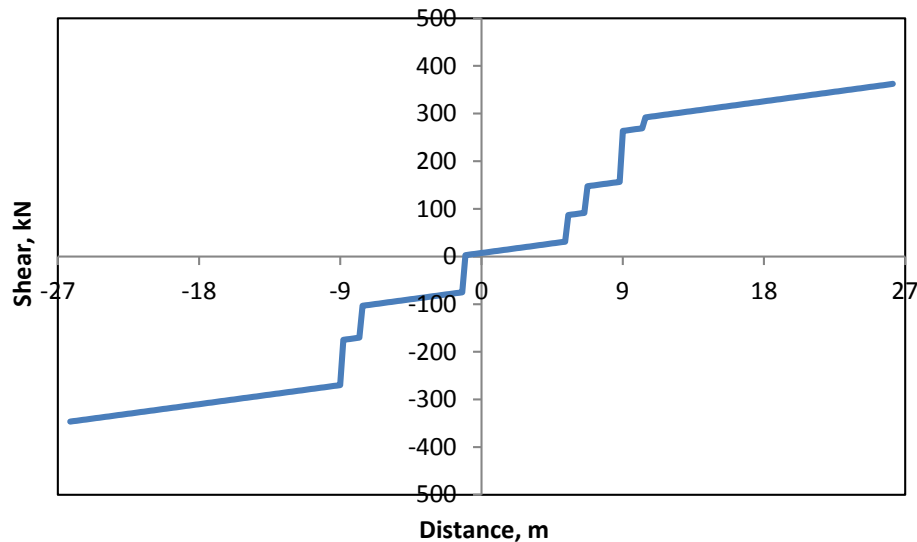

Fig. 7.1: Shear force diagram for determining the loading of the edge due to the critical live loading case for maximum moment at midspan.

The loading from the 3D model was simulated in the 2D model of the exterior girder with a combination of uniform loading on the top, point loads applied at the top to simulate the axle loads and vertical shears applied to the diaphragms. Figure 7.2 shows the live load applied to the model for the controlling load case for maximum moment at midspan. This critical service live loading case results in a moment near midspan of 6,200 kNm.

A shrinkage strain of 0.347 x 10^{-3}, obtained from the 3D analysis, was applied to the concrete.
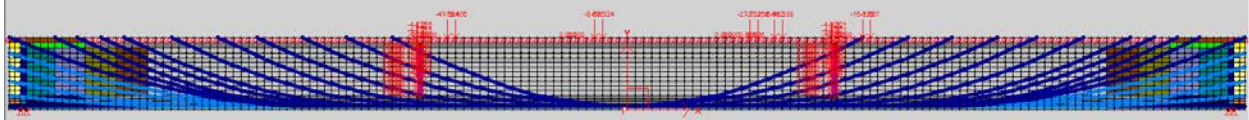
Fig. 7.2: Controlling load case for midspan moment under service live load.

7.2 Evaluation of P7 under Service Load with no Corrosion

As shown in Fig. 7.3, no cracking was predicted under service loading (D + L). First flexural cracking is predicted to occur at a load level of D + 3.1L if the short-term material properties are used in the analysis. For long-term predictions first flexural cracking is predicted to occur at a load corresponding to D + 2.5L.
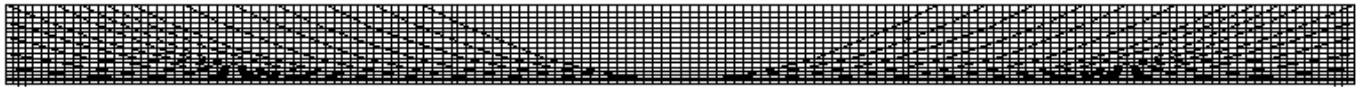
(a) Overall view
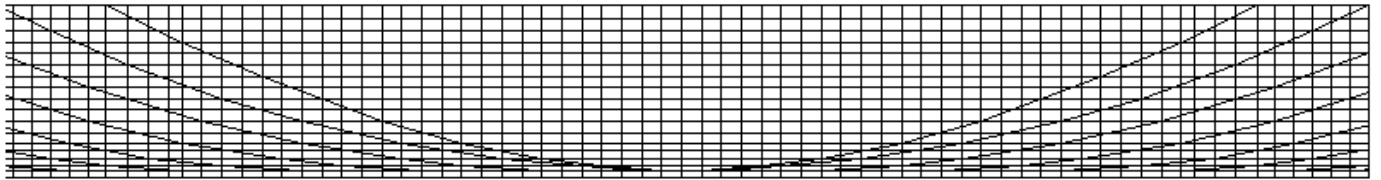
(b) Close-up of midspan region

Fig. 7.3: Conditions of girder under service loads (as originally designed but with concrete compressive strength of 53.9 MPa and no corrosion)

7.3 Evaluation of P7 under Factored Load with No Corrosion

An analysis under factored loading was carried out using material resistance factors for the concrete, reinforcing steel and prestressing steel (see Section 4.2). This analysis uses the conditions of the girder as originally designed but with a concrete compressive strength of 53.9 MPa. No cracking is predicted under factored loading for the critical live loading condition for maximum moment at midspan. The factored loading was equal to:

$$1.09 \times D1 + 1.18 \times D2 + 1.63 \times L$$

In order to assess the maximum factored resistance of girder P7, the live loading was increased incrementally until failure was predicted. Fig. 7.4 shows the conditions of the girder at predicted

19

failure, assuming that there is no corrosion of the reinforcing bars or tendons. It is noted that the girder is predicted to fail in flexure. The predicted flexural cracks extend over the full depth of the web and there is only minor inclined cracking due to shear. This analysis was carried out by first loading the girder with factored dead loads and then increasing the live load to cause failure. The resulting factored loading to cause failure is given by:

$$1.09 \times D1 + 1.18 \times D2 + X \times L$$

Where X is the load factor on the live load, L, to cause failure. From the non-linear analysis this factor was determined to be 3.67. This is greater than the required live load factor of 1.63 for the evaluation of the girder. Another way of expressing the margin of safety is by using the demand/capacity ratio, D/C, which for this case is 0.72.
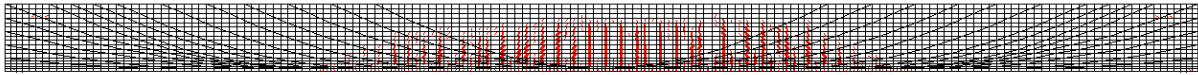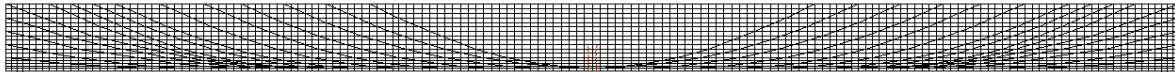

(a) Overall view
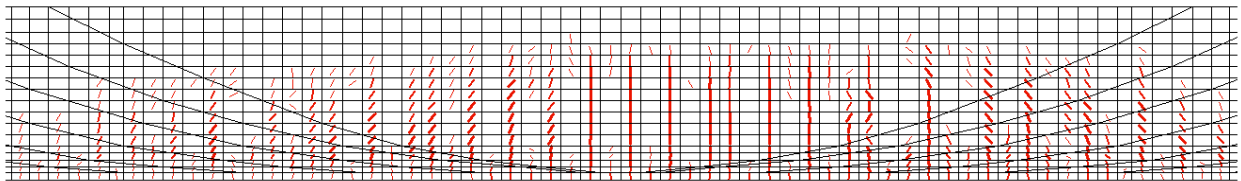
(b) Close-up of midspan region

Fig. 7.4: Conditions of girder at flexural ultimate under 1.39 times factored loads (without corrosion).

7.4 Service Load Predictions with Corroded Tendons and Corroded Stirrups

Figure 7.5 shows the predictions from the non-linear finite element analysis at service load (D+L) for the girder having the degree of corrosion as described in Section 6.2. For this prediction, the short-term stress-strain relationships for the concrete, prestressing tendons and reinforcing steel were assumed. The predicted maximum crack widths are 0.51, 0.74 and 0.45 mm at the bottom of the flange, in the taper of the bottom flange and in the web, respectively. For this short-term prediction, first flexural cracking is predicted to occur at a load of D + 0.5L.
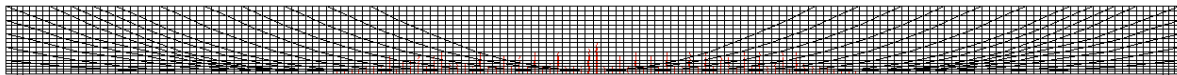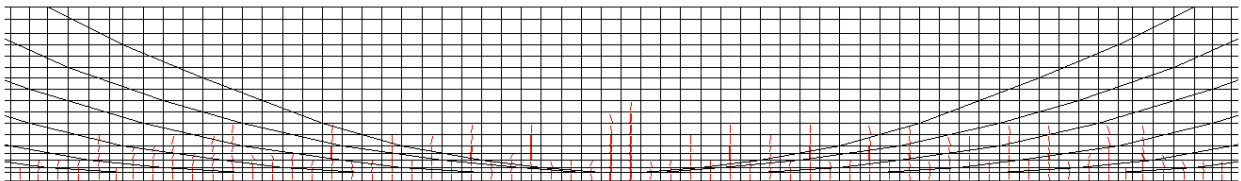

(a) Overall view
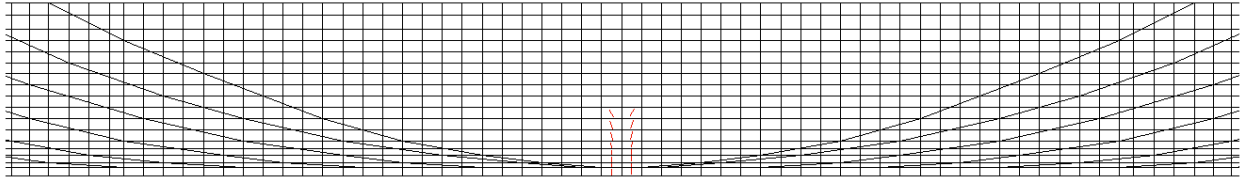
(b) Close-up of midspan region

Fig. 7.5: Predicted short-term conditions of girder at service load (D+L) with 40% uniform corrosion in tendons and stirrups and 46.9% corrosion of tendons at midspan.

A separate non-linear analysis was carried out with long-term properties for the concrete and the prestressing tendons (see Fig. 7.6). These long-term properties result in a loss of prestressing due to the reduced modulus of the prestressing steel and due to the greater strains in the concrete. The predicted long-term crack widths at midspan under service loads for the assumed degree of corrosion are 1.0 mm, 2.0 mm and 1.74 mm at the bottom of the flange, in the taper of the bottom flange and in the web, respectively. The additional flexural cracking outside of the midspan region is due to the loss of effective prestressing due to long-term losses and due to the assumption of a 40% uniform loss of tendons outside of the midspan region . For this case first flexural cracking is predicted to occur at a load of D + 0.3L.

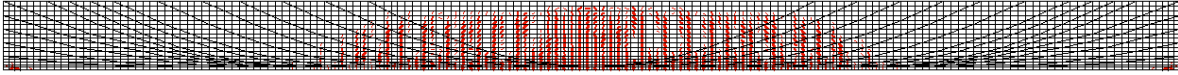(a) Overall view

(b) Close-up of midspan region

Fig. 7.6: Predicted long-term conditions of girder at service load (D+L) with 40% uniform corrosion in tendons and stirrups and 46.9% corrosion of tendons at midspan.

It is noted that the crack widths for girder P7, if no strengthening measures had been implemented, should lie between the short-term and the long-term predicted values.

7.5 Factored Load Predictions with Corroded Tendons and Corroded Stirrups

Fig. 7.7 shows the cracking when the 2-D model reaches the predicted capacity. With the assumed degree of corrosion it is predicted that the beam fails in flexure. The predicted capacity corresponds to the factored dead load plus 1.3 times the service live load. This is somewhat below the factored moment M_f, due to factored dead load and 1.63 times the service live load.

21

This flexural capacity represents 94% of M_f. This corresponds to a demand/capacity ratio, D/C, of 1.06.

(a) Overall view
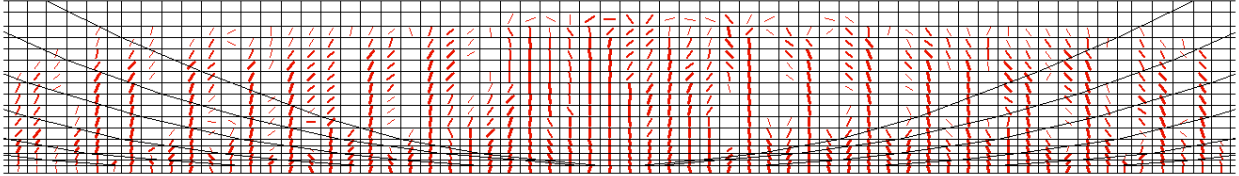
(c) Close-up of midspan region

Fig. 7.7: Predicted cracking at flexural ultimate with simulated corrosion.

8. Predicted Behaviour for Shear Loading Case #1, Without Strengthening Measures

8.1 Loads Applied to the Finite Element Model

The dead loading cases were applied in the same manner as described above. The truck loading was positioned so that girder P7 experienced high shears near the north end of the span.

The governing live load due to traffic for maximum shear near the north end of the girder was determined from the following load case:

- This load case has 3 traffic lanes loaded with lane loads. The lane load consists of 80% of the CL-625 truck plus a uniformly distributed load of ▮ kN/m. Due to the fact that 3 lanes are loaded a modification factor for multiple lane loading equal to 0.80 was applied.
- For lane 1, the rear wheel of the CSA CL-625 truck travelling south is located ▮ m from the centreline of the north support.
- For lanes 2 and 3, the rear wheels of the CSA CL-625 trucks travelling south are located ▮ m from the centreline of the north support. The trucks in these lanes are positioned to cause significant transfer of loads through the diaphragms.

The forces acting on P7 due to this loading were obtained from the 3D analysis. Fig. 8.1 shows the variation of shear force along the length of the girder that was used in the 2D model to simulate the loading obtained from the 3D model.
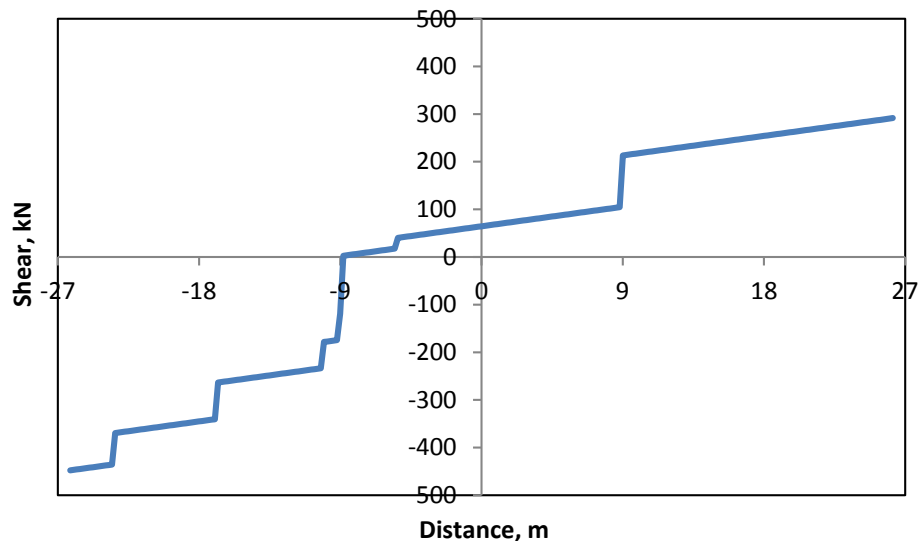

Fig. 8.1: Shear diagram that was used in the 2D model.

The loading from the 3D model was simulated in the 2D model of the exterior girder with a combination of uniform loading on the top, point loads applied at the top to simulate the axle loads and vertical shears applied to the diaphragms (see Fig. 8.2).

A shrinkage strain of 0.347 x 10^{-3}, obtained from the 3D analysis, was applied to the concrete.
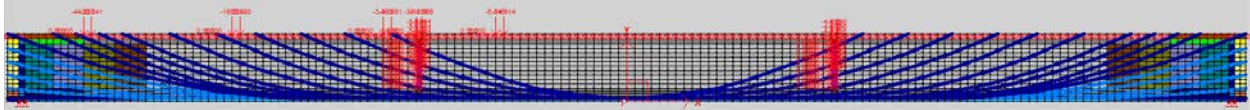

Fig. 8.2: Shear loading Case #1 for service live load.

8.2 Evaluation of P7 under Service Shear Load Case #1, with No Corrosion

This analysis uses the conditions of the girder as originally designed but with a concrete compressive strength of 53.9 MPa. No cracking is predicted under service loading for the shear loading Case #1. First cracking is predicted to occur at a load of D + 3.2L and D+ 2.6L for the short–term and long-term predictions, respectively.
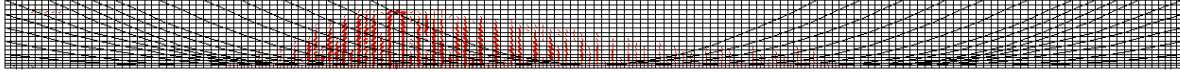
8.3 Evaluation of P7 under Factored Shear Load Case #1, with No Corrosion

No cracking is predicted under factored loading for the critical live loading condition for maximum shear near the north end of P7.

In order to assess the maximum factored resistance of girder P7 for shear loading case #1, the live loading was increased incrementally until failure was predicted. Fig. 8.3 shows the conditions of the girder at predicted failure, assuming that there is no corrosion of the reinforcing bars or tendons. It is noted that the girder is predicted to fail in flexure with the predicted flexural cracks extending over the full depth of the web on either side of the north-interior diaphragm. There is no predicted major inclined cracking due to shear. This analysis was carried out by first loading the girder with factored dead loads and then increasing the live load to cause failure. The resulting factored loading to cause failure is given by:

$$1.09 \times D1 + 1.18 \times D2 + X \times L$$

Where X is the load factor on the live load, L, to cause failure. From the non-linear analysis this factor was determined to be 4.08. This is greater than the required live load factor of 1.63 for the evaluation of the girder. Another way of expressing the margin of safety is by using the demand/capacity ratio, D/C, which for this case is 0.68.
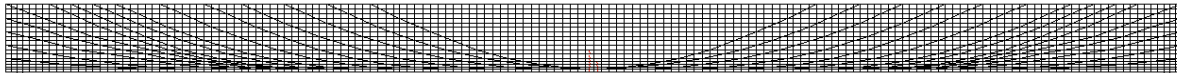
(a) Overall view
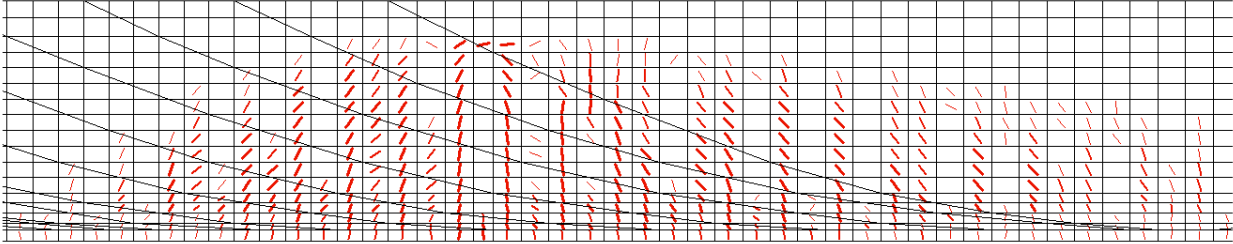
(b) Close-up of failure region

Fig. 8.3: Predicted cracking at flexural ultimate with no corrosion.

8.4 Evaluation of P7 under Service Shear Load Case #1, with Corroded Tendons and Corroded Stirrups

This model also assumed a concentrated loss of 11.25 tendons in the midspan region due to corrosion as described in Section 6.2. A uniform loss of 40% was assumed for the tendons and the vertical stirrups outside of the midspan region.

Fig. 8.4 shows the condition of P7 under service loading for shear Case #1 with simulated corrosion. Flexural cracking appears in the midspan region and no inclined shear cracking is predicted. The predicted crack widths are 0.36, 0.65, 0.40 mm in the bottom of the flange, in the flange taper and in the bottom of the web, respectively. First flexural cracking occurs at loads of D + 0.6L for this short-term loading case.
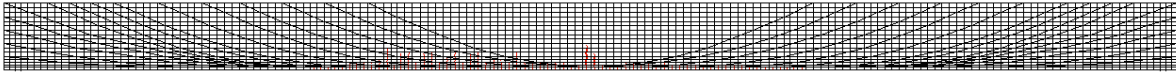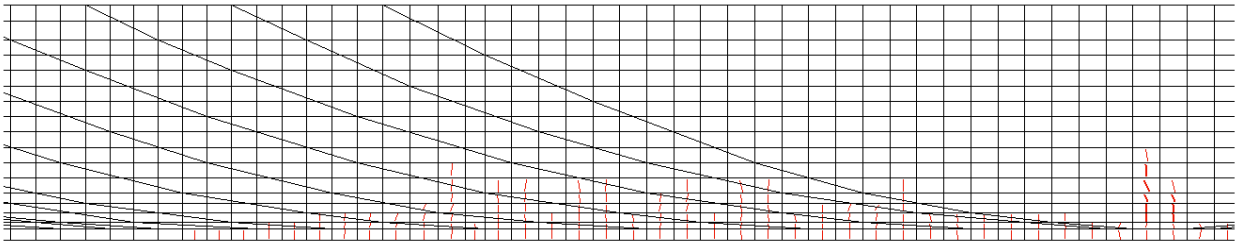

(a) Overall view
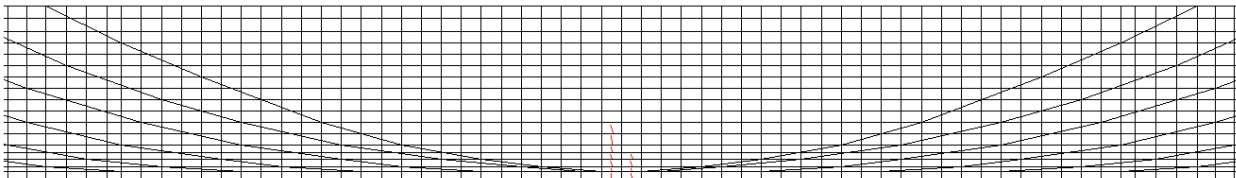
(b) Close-up of cracking near midspan

Fig. 8.4: Predicted cracking at service load level for shear load Case #1, with short-term properties

25

A separate analysis was carried out assuming long-term material properties with corroded tendons and corroded stirrups. Fig. 8.5 shows the condition of P7 under long-term service loading for shear Case #1 with simulated corrosion. The maximum flexural cracks occur near midspan, with flexural cracking occurring over a significant length of the girder. The predicted maximum crack widths are 0.90, 1.52, and 1.43 mm in the bottom of the flange, in the flange taper and in the bottom of the web, respectively. First flexural cracking occurred at a load level of D + 0.4L for this long-term loading case.

(a) Overall view

(b) Close-up of cracking near midspan

Fig. 8.5: Predicted cracking at service load level for shear load Case #1, with long-term properties

8.5 Evaluation of P7 under Factored Shear Load Case #1 with Corroded Tendons and Stirrups

Figure 8.6 shows the predicted cracking at ultimate for shear loading Case #1 with simulated corrosion of the post-tensioning and vertical stirrups. This ultimate case corresponds to a load factor on the lane loading of 1.47 compared with the required load factor of 1.63. This predicted failure load corresponds to about 97% of the required factored load for shear loading case #1. This represents a D/C ratio of 1.03.
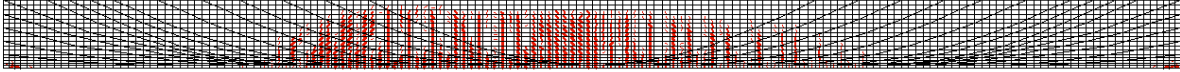
(a) Overall view
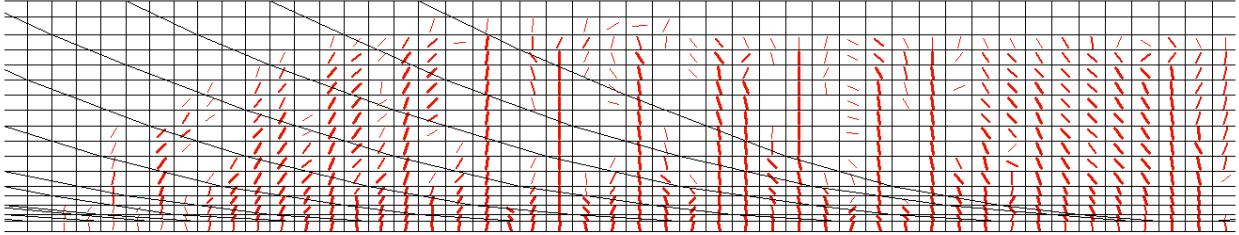
(b) Close-up of critical cracking region

Fig. 8.6: Predicted cracking at ultimate for shear loading Case #1 with corroded tendons and stirrups.

9. Predicted Behaviour for Shear Loading Case #2, without Strengthening Measures

9.1 Loads Applied to the Finite Element Model

The dead loading cases were applied in the same manner as described above. The truck loading was positioned so that the north half of girder P7 experienced high shears and moments near the north-interior diaphragm.

The governing live loading due to traffic for this case was:

- This load case has 3 traffic lanes loaded with lane loads. The lane load consists of 80% of the CL-625 truck plus a uniformly distributed load of ▮ kN/m. Due to the fact that 3 lanes are loaded a modification factor for multiple lane loading equal to 0.80 was applied.
- For lanes 1, 2 and 3, the rear wheel of the CSA CL-625 truck travelling south is located ▮ m from the centreline of the north support.

This loading case results in the centroid of the trucks being approximately at the location of the north-interior diaphragm.

The forces acting on P7 due to this loading were obtained from the 3D analysis. Fig. 9.1 shows the variation of shear force along the length of the girder that was used in the 2D model to simulate the loading obtained from the 3D model.
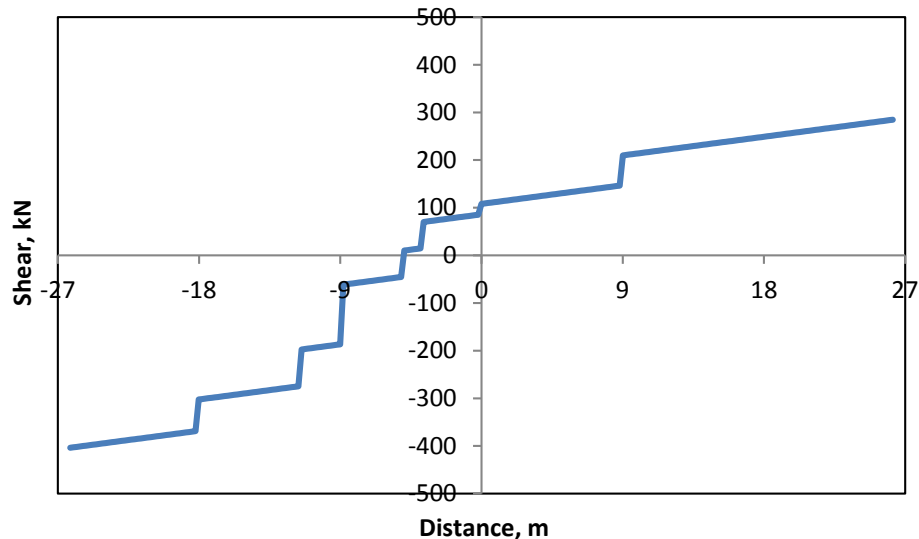

Fig. 9.1: Shear diagram that was used in the 2D model.

Figure 9.2 shows the combination of uniform loading on the top, point loads applied at the top to simulate the axle loads and vertical shears applied to the diaphragms to simulate the live loading

obtained from the 3D analysis. A shrinkage strain of 0.347 x 10^{-3}, obtained from the 3D analysis, was applied to the concrete.
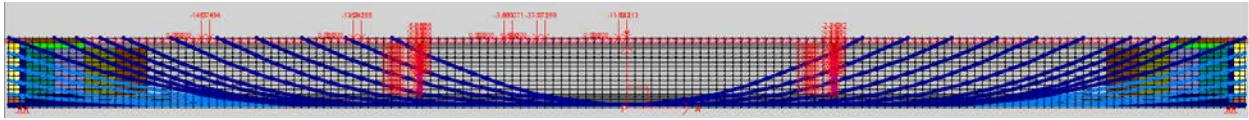

Fig. 9.2: Shear loading Case #2 for service live load.

9.2 Evaluation of P7 under Service Shear Load Case #2, with No Corrosion

This analysis uses the conditions of the girder as originally designed but with a concrete compressive strength of 53.9 MPa. No cracking is predicted under service loading for the shear loading Case #2. First cracking is predicted to occur at loads corresponding to D + 3.1L and D + 2.6L for the short-term and long-term analyses, respectively.

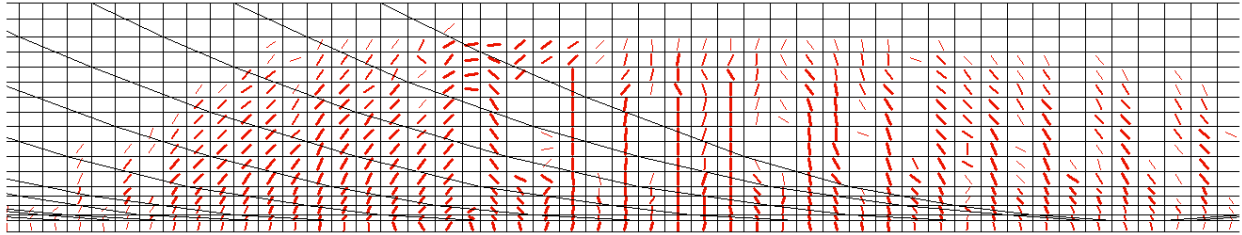## 9.3 Evaluation of P7 under Factored Shear Load Case #2, with No Corrosion

No cracking is predicted under factored loading for the critical live loading condition for maximum shear near the interior-north diaphragm of P7.

Figure 9.3 shows the conditions of the girder at predicted failure, assuming that there is no corrosion of the reinforcing bars or tendons. It is noted that the girder is predicted to fail in flexure with the predicted flexural cracks extending over the full depth of the web on either side of the north-interior diaphragm. Although the failure mechanism is flexural there are some flexure-shear cracks predicted to occur in the region between the support and the interior diaphragm near the north end.

From the non-linear analysis the multiplier on the service live load at this predicted failure was determined to be 4.08. This is considerably greater than the required live load factor of 1.63 for the evaluation of the girder. Another way of expressing the margin of safety is by using the demand/capacity ratio, D/C, which for this case is 0.69.
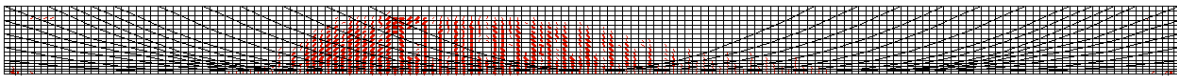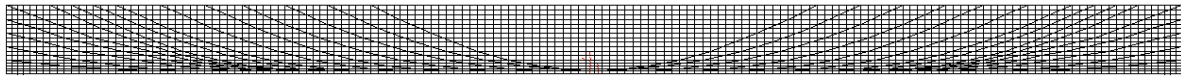

(a) Overall view

(b) Close-up of failure region

Fig. 9.3: Predicted cracking at flexural ultimate for shear loading case #2, with no corrosion.

9.4 Evaluation of P7 under Service Shear Load Case #2, with Corroded Tendons and Corroded Stirrups

An analysis was carried out assuming that 40% of the tendons and 40% of the vertical stirrups were lost due to corrosion. This model also assumed a concentrated loss of 11.25 tendons in the midspan region due to corrosion as described in Section 6.2.

Fig. 9.4 shows the condition of P7 under service loading for shear Case #2 with simulated corrosion. Flexural cracking appears in the midspan region and no inclined shear cracking is predicted. The predicted crack widths are 0.40, 0.79, 0.49 mm in the bottom of the flange, in the flange taper and in the bottom of the web, respectively. First cracking is predicted to occur at a load corresponding to D + 0.6L.

(a) Overall view
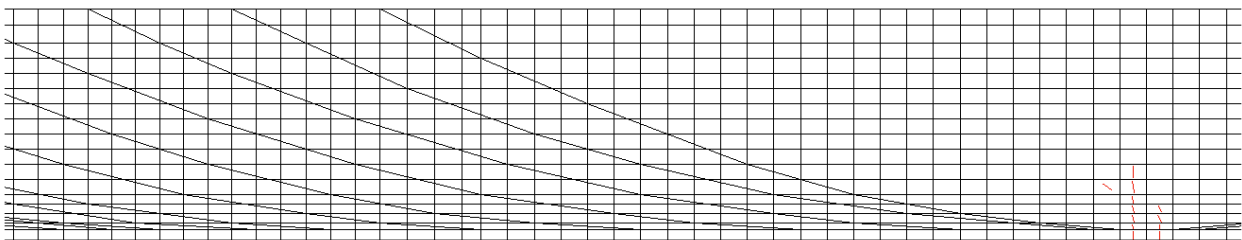
(b) Close-up of cracking near midspan

Fig. 9.4: Predicted cracking at service load level for shear Case #2, with short-term properties

A separate analysis was carried out assuming long-term material properties with corroded tendons and corroded stirrups. Figure 9.5 shows the condition of P7 under long-term service loading for shear Case #2 with simulated corrosion. The maximum flexural cracks occur near midspan, with flexural cracking occurring over a significant length of the girder. The predicted maximum crack widths are 0.97, 2.49, and 2.08 mm in the bottom of the flange, in the flange

30

taper and in the bottom of the web, respectively. First cracking is predicted to occur at a load corresponding to D + 0.4L. It is noted that shear loading case #2 is slightly more critical than shear loading case #1.
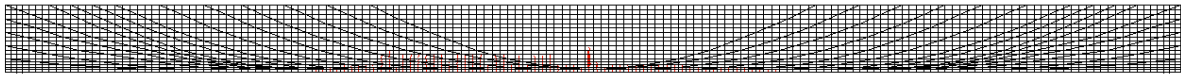

(a) Overall view
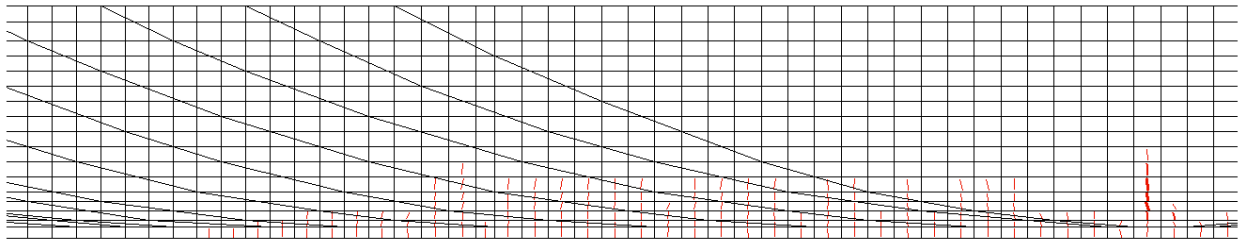
(b) Close-up of cracking near midspan

Fig. 9.5: Predicted cracking at service load level for shear Case #2, with long-term properties.

9.5 Evaluation of P7 under Factored Shear Load Case #2 with Corroded Tendons and Stirrups

Figure 9.6 shows the predicted cracking at ultimate for shear loading Case #2 with simulated corrosion of the post-tensioning and vertical stirrups. This ultimate case corresponds to a load factor on the lane loading of 1.30 compared with the required load factor of 1.63. This predicted failure load corresponds to about 94% of the required factored load for shear loading case #2. This represents a demand to capacity ratio of 1.07.
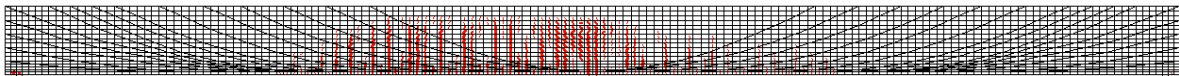
(a) Overall view
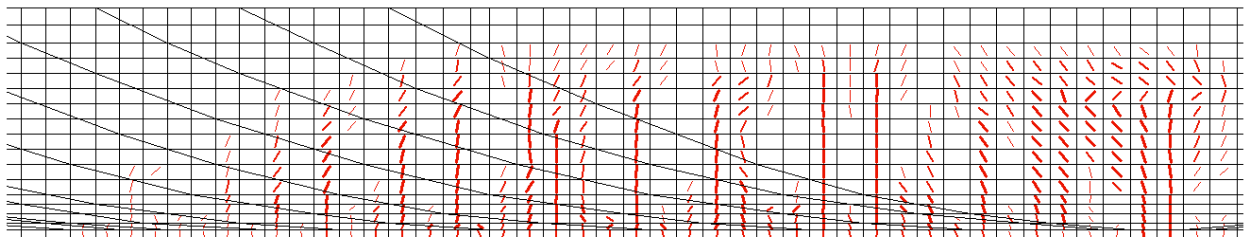
(b) Close-up of critical cracking region

Fig. 9.6: Predicted cracking at ultimate for shear Case #2 with corroded tendons and stirrups.

10.   Predicted Behaviour of Girder P7, with External Post-Tensioning (PTE)

10.1   Introduction

Due to the fact that the behaviour of girder P7, without strengthening measures, is governed by flexural cracking at service load and by flexural failure at ultimate load, the analysis in this section will examine the case of maximum moment at midspan.

It is interesting to appreciate the history of the design and application of the external post-tensioning (PTE) on girder P7 of span 28W-29W. From the calculations reported by Les Consultants S.M. Inc (SM, 1999) it was assumed in 1998 that due to corrosion in girder P7 that 3.1 tendons had been lost due to corrosion. At that time the stress conditions of P7 at midspan were determined with the following assumptions:

- Only 20.91 of the 24 tendons were effective
- A QS 660 truck loading was assumed
- Losses in the PTE were neglected
- 100% of the applied PTE was considered to act on girder P7

The level of PTE was chosen such that with the lost tendons and the assumed effectiveness of the PTE, there would be no tension in the bottom fibre under service loading. Although the service load moment assumed in these calculations was about 8.4% higher than that used in this study, more tendons corroded with time and more detailed analysis revealed that the PTE was not 100% effective on girder P7.

 In 1998 only girder P7 of span 28W-29W was strengthened using external post-tensioning applied at the level of the bottom flange (see Fig. 10.1). A total of 8 - 15mm diameter strands (4 on each side of girder P7) were installed. These strands, with an ultimate strength, f_{pu}, of 1860 MPa, were initially stressed to $0.6f_{pu}$. From the analysis carried out using CSI Bridge it was determined that after all losses this stress would reduce to $0.54f_{pu}$. This gives a total prestressing force after all losses of:

$$P_{final} = 8 \times 140 \times 0.54 \times 1860 = 1125 \ \text{kN}$$

It is noted that at this time (1998) the PTE was applied only to P7 and not to P1 in span 28W-29W.
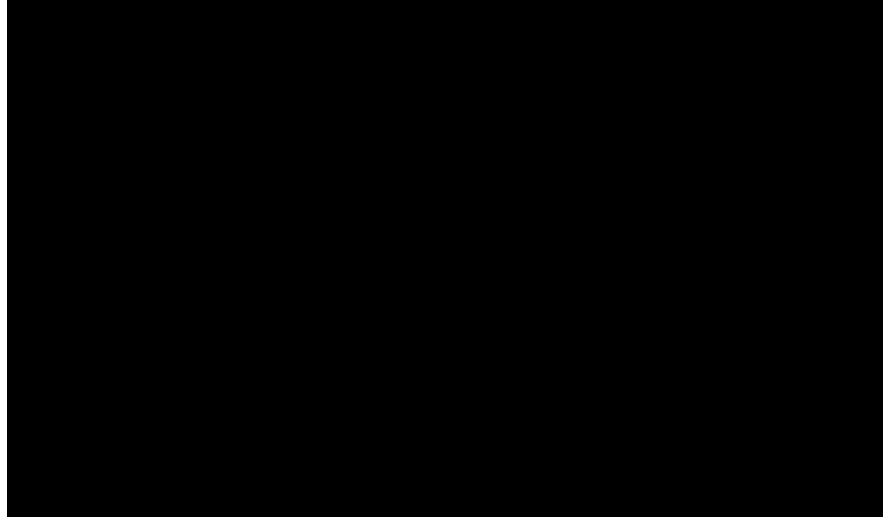
Fig. 10.1: Details of PTE for girder P7 in span 28W-29W added in 1998 (PJCCI drawing 125101-06, 1998).

It is noted that the 3D analysis that was carried out indicates that with this tendon force applied to P7 only, the effective axial force in girder P7 at midspan was 565 kN. This means that only about 50% of the applied PTE is active at midspan of girder P7. This loss of PTE in girder P7 is due to the significant spreading of compression that occurs in the superstructure.

From the structural drawings of AECOM (2011) it was determined that a different level of PTE was added to girder P1 of span 28W-29W in the period 2012-2013. The drawings show that a total of 18 - 15mm diameter strands (9 on each side of girder) were installed on girder P1 (see Fig. 10.2). The total assumed prestressing force after all losses was:

$$P_{final} = 18 \times 140 \times 0.54 \times 1860 = 2531 \text{ kN}$$
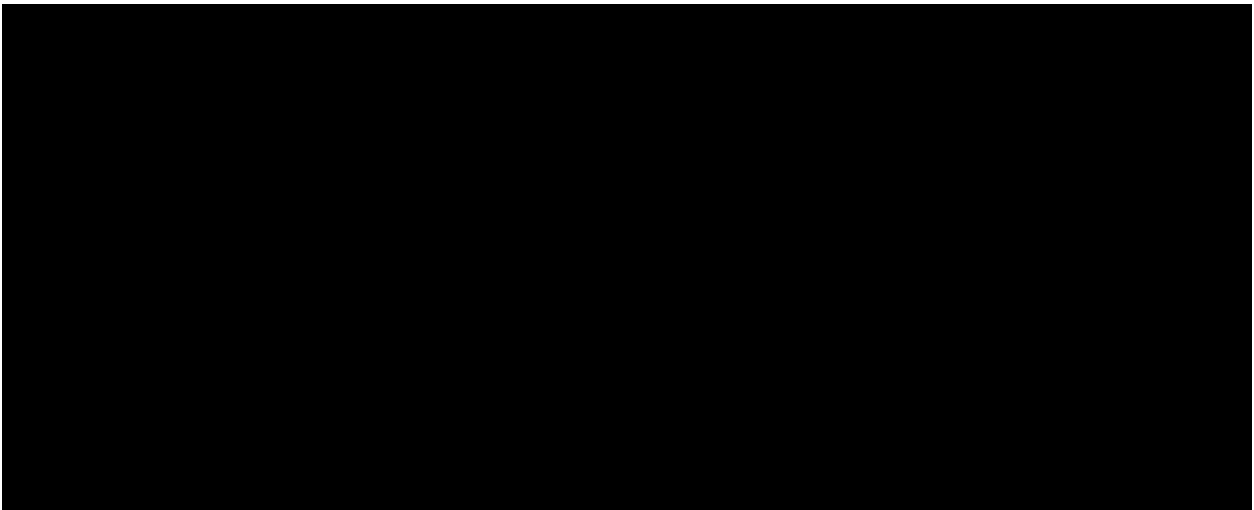

Fig. 10.2: Details of PTE for girder P1 in span 28W-29W added in 2012 (AECOM, drawing 125570 -32, 2012).

The 3D analysis indicates that the effect of adding PTE to girder P1 is to induce tension in girder P7. If the combined effect of the PTE on girder P7 and P1, as described above, is considered

then, from the 3D analysis, the effective axial compression on P7 is reduced to 230 kN. It is assumed that both of these PTE levels were applied to span 28W-29W and were present when the severe cracking was observed in 2013.

Figure 10.3 shows the axial force and shear force diagrams corresponding to the forces applied to the 2D model of girder P7 to simulate the external horizontal post-tensioning. Figure 10.4 shows the forces applied to the 2D model to simulate the effects of PTE on P7.
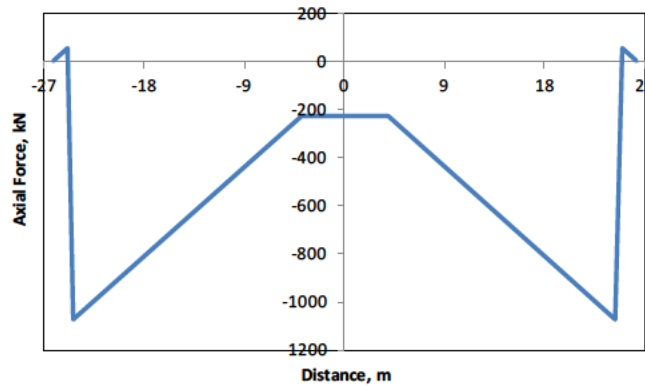
(a) Axial force
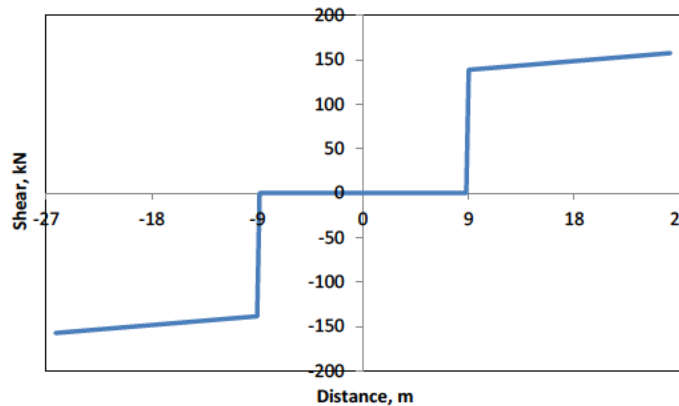
(b) Shear force

Fig. 10.3: Axial force and shear force diagrams corresponding to the forces applied to the 2D model of girder P7 to simulate the external horizontal post-tensioning.

Fig. 10.4 Forces applied to girder P7 to simulate the PTE.

34

10.2 Behaviour of Girder P7 due to Service Loading, with Corrosion and PTE
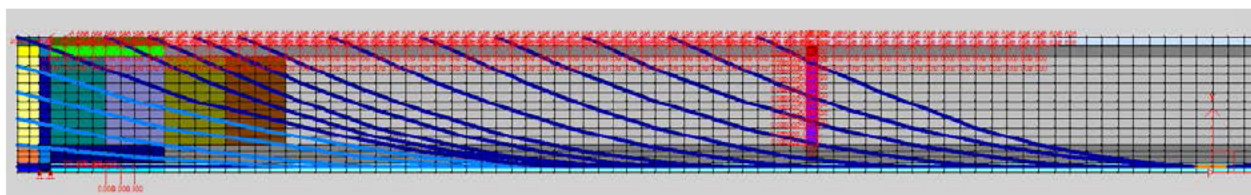
Figure 10.5 shows the predicted cracking in the midspan region for girder P7 with corroded tendons and corroded stirrups after the external post-tensioning has been applied. Short-term material properties were used in making this prediction. It is noted that the application of these two different levels of PTE in P1 and P7 did not prevent cracking. The predicted maximum crack widths are 0.42, 0.60, and 0.32 mm in the bottom of the flange, in the flange taper and in the bottom of the web, respectively. First cracking is predicted to occur at a load corresponding to D + 0.6L.
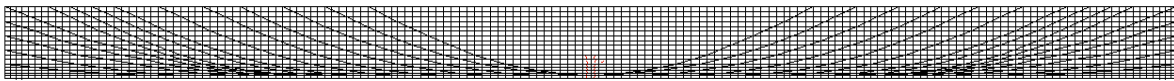
(a) Overall view
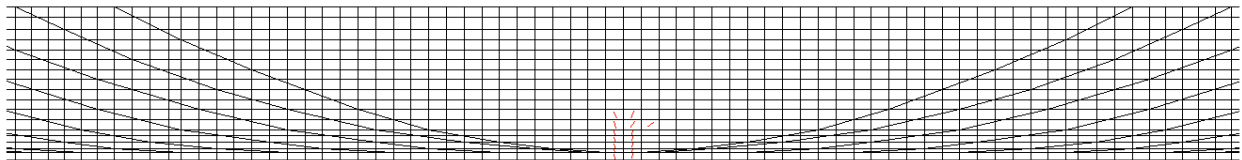
(b) Close-up of midspan region

Fig. 10.5: Cracking predictions for maximum moment at midspan for short-term service loads with corroded tendons and corroded stirrups, strengthened with PTE.

Figure 10.6 shows a similar prediction, but with long-term material properties. The predicted maximum crack widths are 0.97, 1.68, and 1.26 mm in the bottom of the flange, in the flange taper and in the bottom of the web, respectively. First cracking is predicted to occur at a load corresponding to D + 0.4L.
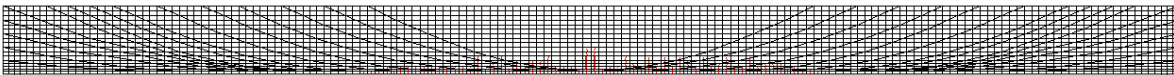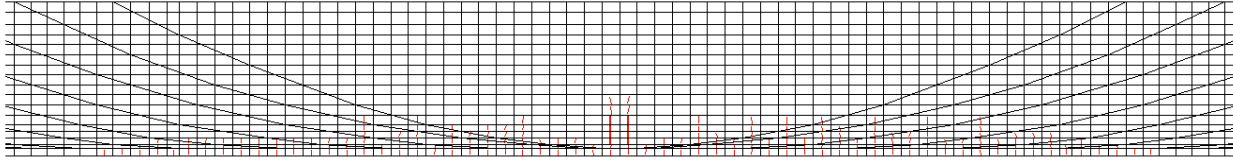

(a) Overall view

(b) Close-up of midspan region

Fig. 10.6: Cracking predictions for maximum moment at midspan for long-term service loads with corroded tendons and corroded stirrups, strengthened with PTE.

10.3   Behaviour of Girder P7 due to Factored Loading, with Corrosion and PTE

Figure 10.7 shows the condition of girder P7 at maximum predicted factored resistance for the live loading case causing maximum moment at midspan with corroded tendons and corroded stirrups, strengthened with PTE.

The girder is predicted to fail in flexure with very large cracks near midspan and flexural cracks occurring over a length of about one-third of the span. Inclined cracking was also predicted near the diaphragms. Failure is predicted at a live load corresponding to a live load factor of 1.47, somewhat below the 1.63 required. The D/C ratio is 1.03.
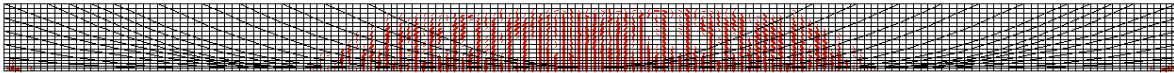
(a) Overall view
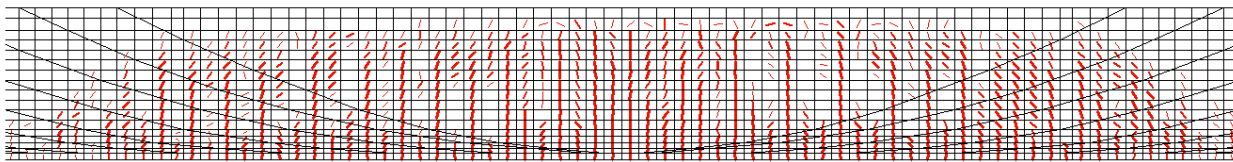
(b) Close-up of midspan region

Fig. 10.7: Predicted factored resistance for maximum moment at midspan with corroded tendons and corroded stirrups, strengthened with PTE.

36

11.   Predicted Behaviour of Girder P7, with Queen Post 1 (QP1) Strengthening

11.1   Introduction

Although girders in some spans were strengthened using the Queen Post 1 method, this strengthening measure was not applied to span 28W-29W. However, an analysis of girder P7 with the application of QP1 was carried out to determine the effects on the response of a girder suffering the same degree of corrosion as that assumed in span 28W-29W.

Figure 11.1 shows the general aspects of the strengthening using QP1 (AECOM 2011). The post-tensioning consisted of 4 - 36 mm diameter high-strength bars (1035 MPa ultimate strength) on each external girder, P1 and P7.
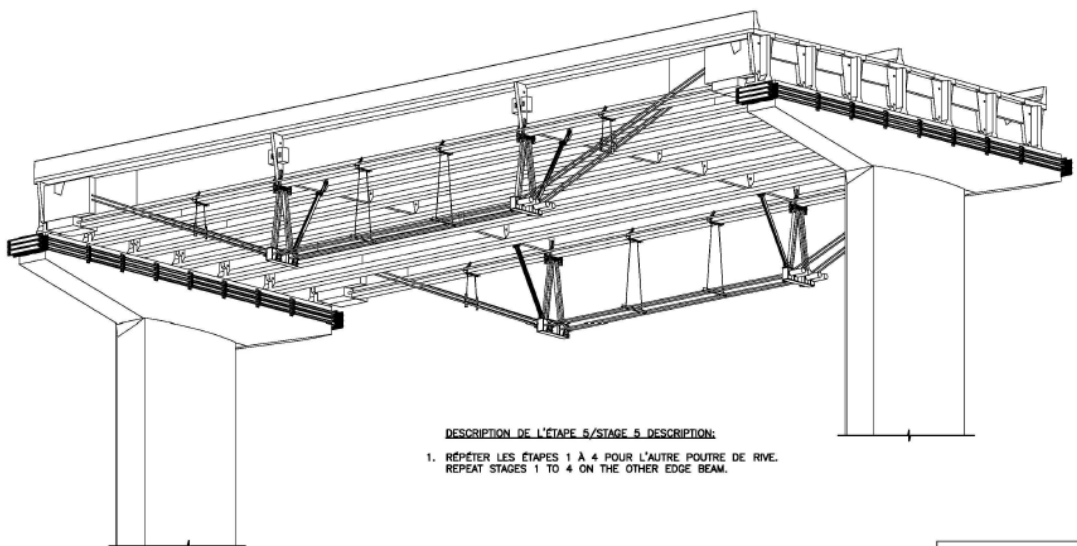
Fig. 11.1: Queen Post 1 Strengthening (AECOM 2011)

In 2009 span 34W-35W was strengthened using QP1 and the stressing records (Construction Euler Inc. 2009) indicated that the desired force per high-strength bar was 475 kN. In order to study the effects of QP1 that had been used in 2009 the total force in the 4 horizontal high-strength bars was assumed to be 4 x 475 kN = 1900 kN. It is noted that the QP1 was added in 2009 and the PTE was added later in 2011 in this span.

A typical span was modelled using the 3D model and the resulting forces applied to girder P7 were used to apply forces in the 2D model. Due to the large forces anchored in the web of the girder near its end, the designers thickened the web over its full height and over a length of about 3.5m. This anchorage block region was simulated in the 2D non-linear model by thickening the web in this region.

37

The analyses were carried out for the critical live loading case corresponding to maximum moment near midspan.

It is noted that the structural drawings for subsequent strengthening using QP1 show a variety of stressing levels depending on the level of PTE, the assumed degree of corrosion and the concrete strength of the diaphragms (see Fig. 11.2). These jacking forces are typically smaller than those used in 2009 on span 34W-35W.

ÉTAT DE LA POUTRE DE RIVE EDGE BEAM CONDITION		RÉSISTANCE EN COMPRESSION f'c DU BÉTON DES DIAPHRAGMES DIAPHRAGM CONCRETE COMPRESSIVE STRENGTH f'c (MPa)				
TENSION DE PRÉCONTRAINTE EXTÉRIEURE LONGITUDINALE EXISTANTE EXISTING EXTERIOR LONGITUDINAL PRESTRESSING LOAD	QUANTITÉ DE CÂBLES INTERNES PERDUS* QUANTITY OF INTERNAL CABLES LOST*	30	35	40	45	>50
1874kN	0	275	350	375	400	425
1874kN	2	300	350	375	400	425
1874kN	4	335	375	375	415	425
2344kN	4	300	335	350	375	400
2344kN	6	325	335	360	375	400
2812kN	6	285	310	325	340	350
2812kN	8	300	325	335	350	360
3281kN	8	260	275	315	315	335
3281kN	10	275	285	315	325	335

TENSION FINALE (T) (kN) PAR BARRE DE PRÉCONTRAINTE HORIZONTALE
(APRÉS PERTES INSTANTANÉES)
FINAL JACKING FORCE (T) (kN) PER HORIZONTAL PRESTRESSING BAR
(AFTER INSTANTANEOUS LOSSES)

Fig. 11.2: Jacking forces used in 2012-2013 for spans strengthened with QP1 AECOM drawing 1255570-47, 2011).

An additional important aspect is that the QP1 was typically applied to girders that already had some form of PTE. The level of PTE also varies depending on the condition of the girder and the date when the strengthening was carried out.

The 2D non-linear analysis to study the effects of QP1 was carried out for the following conditions:

- A degree of corrosion in girder P7 with corroded tendons and corroded stirrups corresponding to that assumed in span 28W-29W,
- The case of QP1 alone, without PTE, and
- The force level that was used in span 34W-35W in 2009.

Figure 11.3 shows the axial load and shear force diagrams corresponding to the loading applied to girder P7 due to QP1.
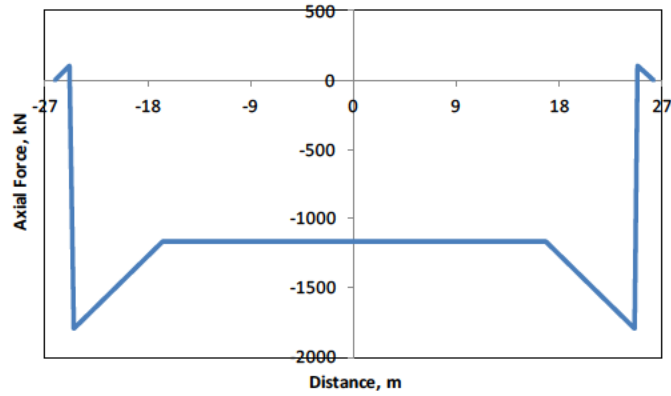
(a) Axial force
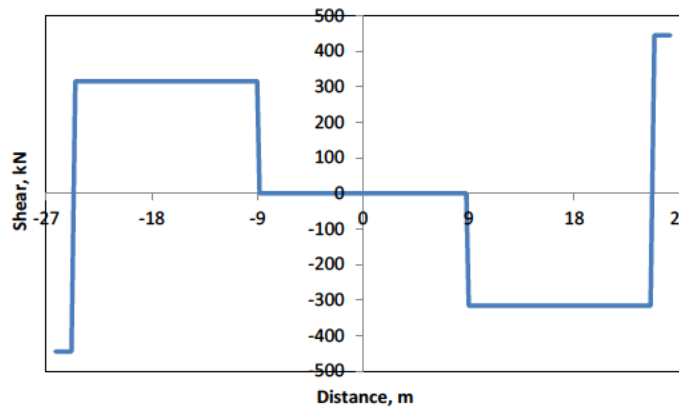
(b) Shear force

Fig. 11.3: Axial load and shear force diagrams corresponding to the loading applied to girder P7 due to QP1.

Figure 11.4 shows the unit loading case (1000 kN) used to simulate the effects of QP1 on girder P7.

Fig. 11.4: Unit loading case used to simulate the effects of QP1 on girder P7.

11.2 Behaviour of Girder P7 due to Service Loading, with Corrosion and QP1

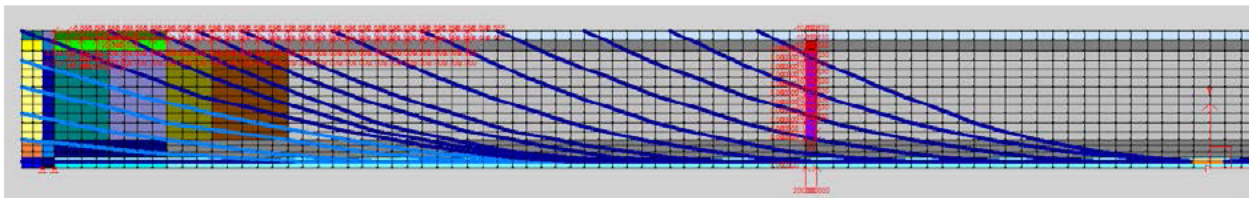The analysis with the corroded tendons and corroded stirrups indicates that under full service loading no cracks were predicted. For the analysis using short-term material properties, first flexural cracking was predicted to occur at a load of D + 1.3L. For analysis using long-term properties first flexural cracking was predicted to occur at a service load of D + 1.1L.

11.3 Behaviour of Girder P7 due to Factored Loading, with Corrosion and QP1

Figure 11.5 shows the ultimate condition of a typical girder P7 with corroded tendons and corroded stirrups and strengthened with QP1.

Failure is predicted to occur at a live load factor of 2.20 which is greater than the required factor of 1.63. The demand-to-capacity ratio, D/C, is 0.95.
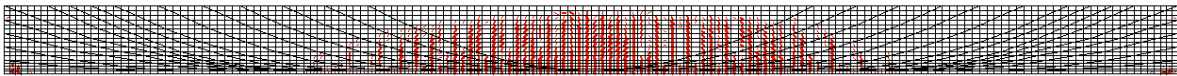
(a) Overall view
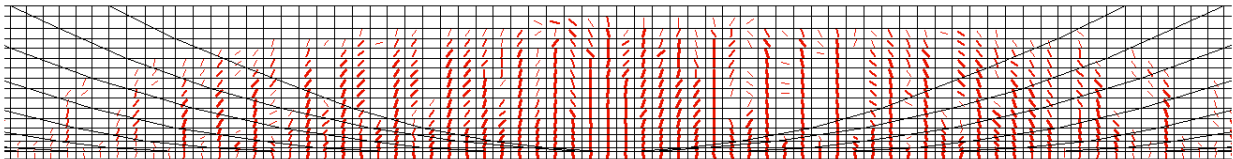
(b) Close-up of middle third of girder

Fig. 11.5: Ultimate condition of typical girder P7 with corrosion and with QP1 strengthening.

12. Predicted Behaviour of Girder P7, with Queen Post 2 (QP2) Strengthening

12.1   Introduction

Although girders in some spans were strengthened using the Queen Post 2 method, this strengthening measure was not applied to span 28W-29W.

In order to study the effect of QP2, an analysis of girder P7 with the application of QP2 forces was carried out to determine the effects on the response of a girder suffering the same degree of corrosion as that assumed in span 28W-29W.

Figure 12.1 shows the general aspects of the strengthening using QP2 (AECOM 2011). The post-tensioning consisted of 16 pairs of 15.2 mm diameter strands (area of 140 mm^2) having an ultimate strength of 1860 MPa (ASTM A416) on each edge girder, P1 and P7.
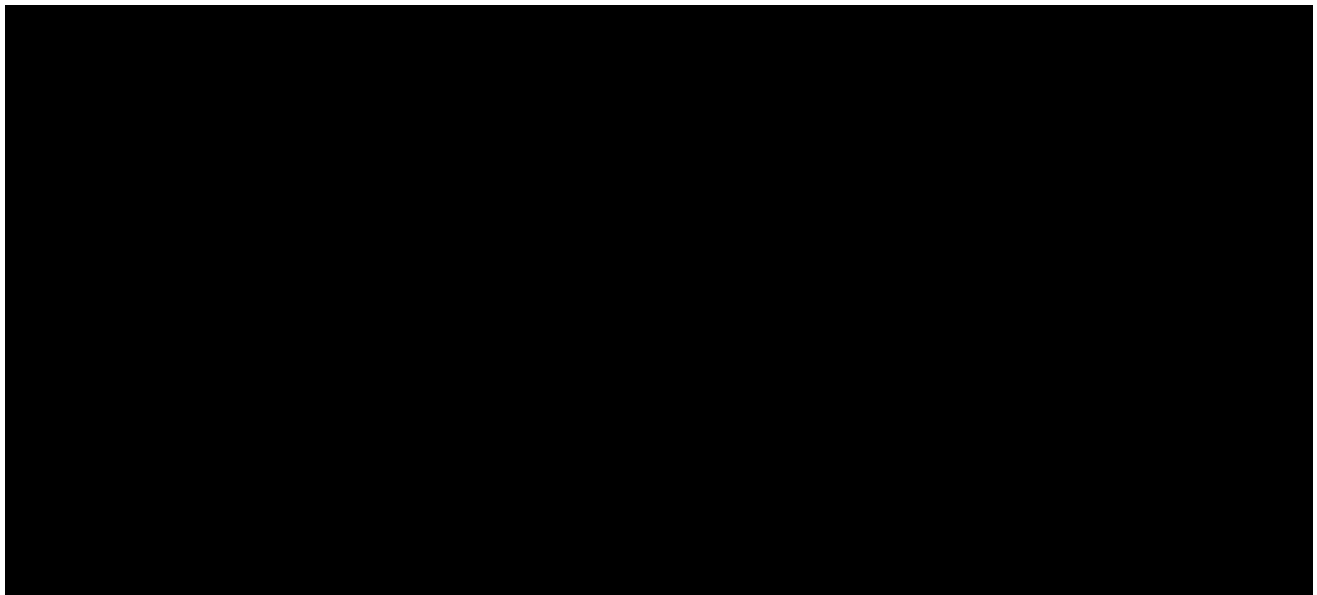

Fig. 12.1: Strengthening details for QP2 (AECOM drawing 1255570-49, 2011).

The 2011 AECOM drawings give jacking force levels in each strand as a function of the degree of corrosion assumed, the level of PTE and the concrete strength of the interior diaphragms (see Fig. 12.2).

ÉTAT DE LA POUTRE DE RIVE EDGE BEAM CONDITION		# DE NOUVEAU MONOTORON NEW SINGLE STRAND	RÉSISTANCE EN COMPRESSION f'c DU BÉTON DES DIAPHRAGMES DIAPHRAGM CONCRETE COMPRESSIVE STRENGTH f'c (MPa)				
TENSION DE PRÉCONTRAINTE EXTÉRIEURE LONGITUDINALE EXISTANTE EXISTING EXTERIOR LONGITUDINAL PRESTRESSING LOAD	QUANTITÉ DE CÂBLES INTERNES PERDUS* QUANTITY OF INTERNAL CABLES LOST*		30	35	40	45	> 50
1874 kN	0	1 @ 4 5 @ 8 9 @ 12 13 @ 16	80 kN	95 kN	105 kN	120 kN	130 kN
1874 kN	2	1 @ 4 5 @ 8 9 @ 12 13 @ 16	80 kN	95 kN	105 kN	120 kN	130 kN
1874 kN	4	1 @ 4 5 @ 8 9 @ 12 13 @ 16	80 kN	95 kN	105 kN	120 kN	130 kN
2344 kN	4	1 @ 4 5 @ 8 9 @ 12 13 @ 16	80 kN	95 kN	105 kN	120 kN	130 kN
2344 kN	6	1 @ 4 5 @ 8 9 @ 12 13 @ 16	80 kN	95 kN 105 kN	105 kN	120 kN	130 kN

TENSION FINALE (T) PAR MONOTORON
(APRÉS PERTES INSTANTANÉES)

ÉTAT DE LA POUTRE DE RIVE EDGE BEAM CONDITION		# DE NOUVEAU MONOTORON NEW SINGLE STRAND	RÉSISTANCE EN COMPRESSION f'c DU BÉTON DES DIAPHRAGMES DIAPHRAGM CONCRETE COMPRESSIVE STRENGTH f'c (MPa)				
TENSION DE PRÉCONTRAINTE EXTÉRIEURE LONGITUDINALE EXISTANTE EXISTING EXTERIOR LONGITUDINAL PRESTRESSING LOAD	QUANTITÉ DE CÂBLES INTERNES PERDUS* QUANTITY OF INTERNAL CABLES LOST*		30	35	40	45	> 50
2812 kN	6	1 @ 4 5 @ 8	80 kN	95 kN	105 kN	105 kN	105 kN
		9 @ 12 13 @ 16	105 kN	105 kN		130 kN	130 kN
2812 kN	8	1 @ 4 5 @ 8	80 kN	95 kN	105 kN	105 kN	105 kN
		9 @ 12 13 @ 16	105 kN	105 kN		130 kN	130 kN
3281 kN	8	1 @ 4 5 @ 8	80 kN	95 kN	105 kN	105 kN	105 kN
		9 @ 12 13 @ 16	105 kN	105 kN		130 kN	130 kN
3281 kN	10	1 @ 4 5 @ 8	80 kN	95 kN	105 kN	105 kN	105 kN
		9 @ 12 13 @ 16	105 kN	105 kN		130 kN	130 kN

* CETTE QUANTITÉ NE POURRA ÊTRE CONFIRMÉE QU'AU MOMENT DE LA RÉFECTION DE LA POUTRE (PHASE DE DÉMOLITION). IL SERA ALORS DÉTERMINÉ PAR L'INGÉNIEUR SI UN RENFORCEMENT EN CISAILLEMENT DE LA POUTRE EST REQUIS (VOIR DESSIN 125570-30).

* THIS QUANTITY SHALL ONLY BE CONFIRMED AT THE MOMENT OF THE BEAM REPAIRS (DEMOLITION PHASE). AT THAT MOMENT THE ENGINEER SHALL DETERMINE IF A BEAM SHEAR REINFORCEMENT IS REQUIRED (SEE DRAWING 125570-30)

Fig. 12.2: Jacking forces used in 2012-2013 for spans strengthened with QP2 (AECOM drawing 1255570-53, 2011).

For this analysis of the effects of QP2 strengthening, the following conditions were assumed:

- A degree of corrosion in girder P7 with corroded tendons and corroded stirrups corresponding to that assumed in span 28W-29W,
- The case of QP2 alone, without PTE,
- The force level that was indicated for use with 10 strands lost due to corrosion and a concrete strength in the diaphragm of at least 40 MPa.
- The jacking force level assumed was 105 kN per strand.

A typical span was modelled using the 3D model and the resulting forces applied to girder P7 were used to apply forces in the 2D model. Due to the large forces anchored in the web of the girder near its end, the designers thickened the web as shown by the shaded areas in Fig. 12.1. This anchorage block region was simulated in the 2D non-linear model by thickening the web in this region.

Figure 12.3 shows the axial load and shear force diagrams corresponding to the loading applied to girder P7 due to QP2.

42
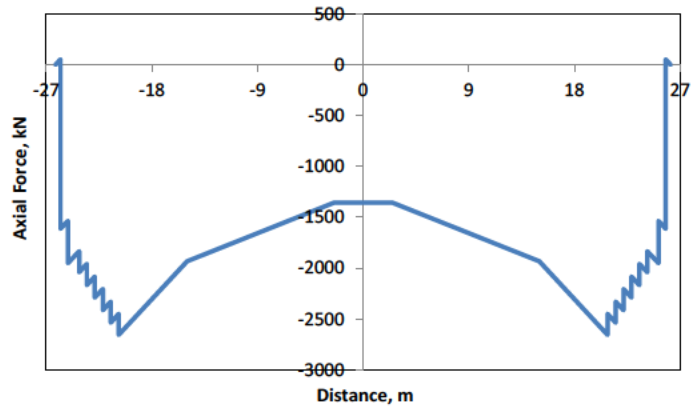
(a) Axial force
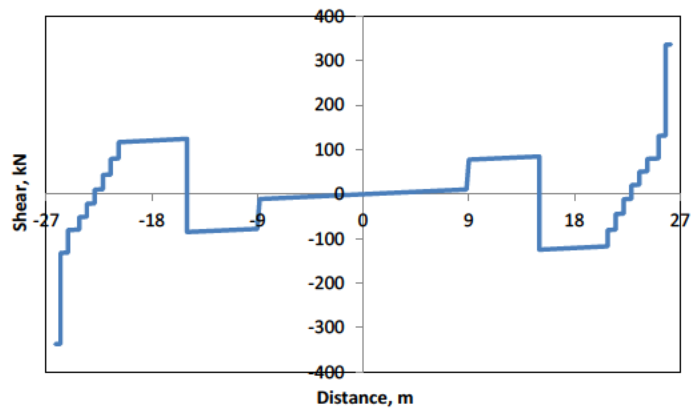
(b) Shear force

Fig. 12.3: Axial load and shear force diagrams corresponding to the loading applied to girder P7 due to QP2.

Figure 12.4 shows the loading used to simulate the effects of QP2 on girder P7. The pink elements shown in Fig. 12.4 indicate the thickening of the web at the anchorage region of the post-tensioning.
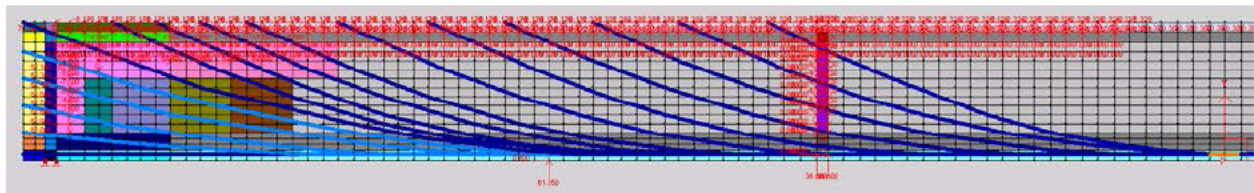

Fig. 12.4: Loading case used to simulate the effects of QP2 on girder P7.

12.2   Behaviour of Girder P7 due to Service Loading, with Corrosion and QP2

The 2D non-linear analysis of girder P7 with short-term material properties does not result in any predicted cracks at service load level. First cracking is predicted to occur at a load of D + 1.1L.

Figure 12.5 shows the predicted cracking that occurs in girder P7 due to the service load level (D + L) for the case of long-term material properties. The predicted crack widths are 0.40 mm for the bottom flange and the flange taper, with no cracking predicted in the web. First cracking is predicted to occur at a load corresponding to D + 0.8L.
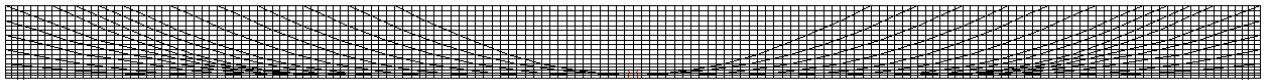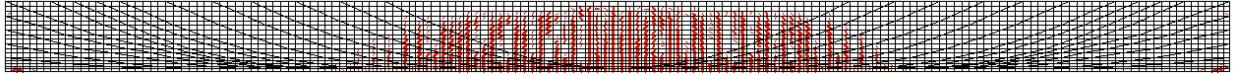

(a) Overall view
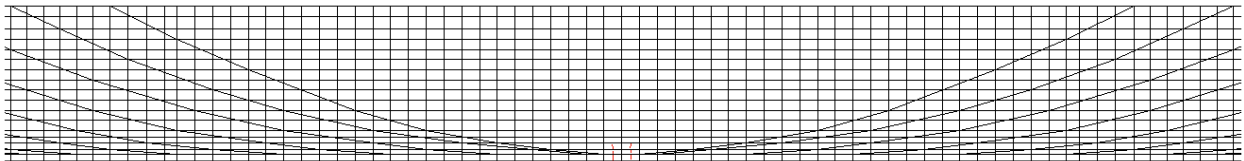
(b) Close-up of midspan region

Fig. 12.5: Predicted cracking using long-term material properties for the case of corroded tendons and corroded stirrups and QP2.

12.3   Behaviour of Girder P7 due to Factored Loading, with Corrosion and QP2

Figure 12.6 shows the condition of girder P7 at ultimate. . The resulting factored loading to cause failure is given by:

$$1.09 \times D1 + 1.18 \times D2 + X \times L$$

Where X is the load factor on the live load, L, to cause failure. From the non-linear analysis this factor was determined to be 1.96. This is greater than the required live load factor of 1.63 for the evaluation of the girder. This results in a demand/capacity ratio, D/C, which for this case is 0.95.

(a) Overall view
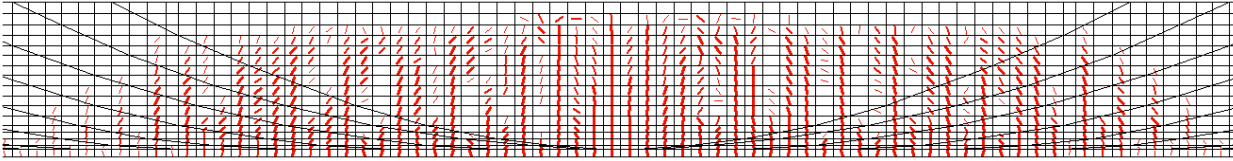
(b) Close-up of midspan region

Fig. 12.6: Predicted flexural failure in girder P7 for corroded tendons and corroded stirrups and QP2.

13.   Summary and Conclusions

13.1   Assessment of Original Design

It is concluded that girder P7 would not experience cracking at service load level and would have significant reserve of strength if no corrosion had taken place. For this assessment a concrete compressive strength of 53.9 MPa was assumed.

It is concluded that the original design would have adequate behaviour at service load, without cracking, and would have adequate flexural and shear strength.

13.2   Simulating Corrosion in P7 in Span 28W-29W

It was concluded that 11.25 tendons, out of the original 24 tendons, were corroded in the midspan region based on inspection and evaluation by the consultants. This led to the use of a 2D non-linear analysis model of girder P7 simulating 46.9% corrosion in the midspan region and a lesser corrosion level of 40% for the tendons and the stirrups outside of this region.

This analytical model resulted in a concentration of predicted cracks in the midspan region, as was observed in girder P7 in November 2013.

13.3   Predicted Behaviour of Girder P7 with Simulated Corrosion and Without Strengthening Measures

Both the sectional analysis and the 2D non-linear finite element analyses predict significant cracking at service load level. Figure 13.1 compares the predicted midspan crack widths using a sectional analysis approach and using the non-linear finite element model. The predictions using the finite element model results in larger predicted crack widths when 11.25 tendons are assumed to be lost due to corrosion.
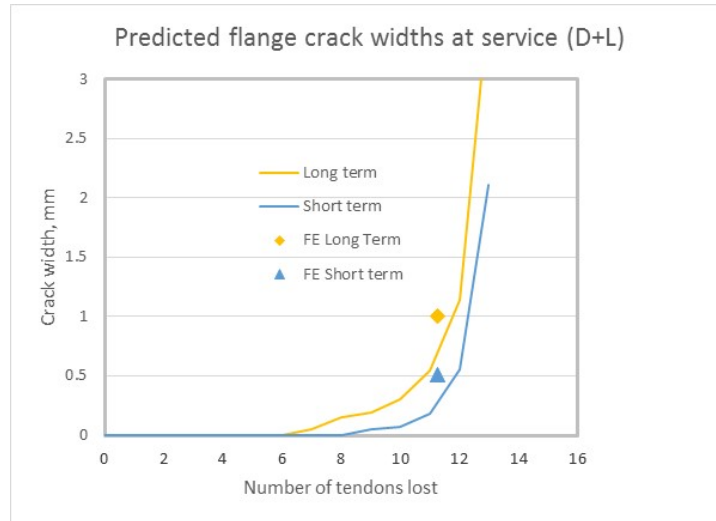
(a) Bottom flange crack widths
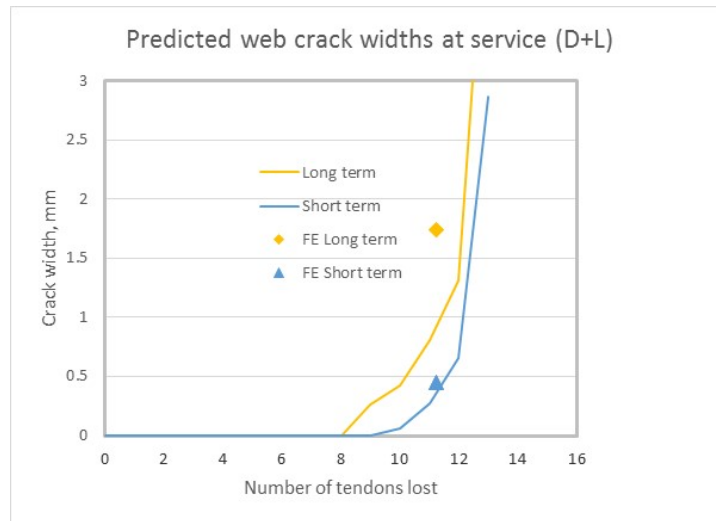
(b) Web crack widths

Fig. 13.1: Comparison of maximum predicted midspan crack widths at service load level using a sectional analysis and using the non-linear finite element model.

Figure 13.2 shows the influence of the degree of corrosion on the factored flexural resistance. It is concluded that, when 10 tendons are lost due to corrosion the factored resistance equals the factored load and when 13 tendons are lost due to corrosion the factored resistance equals the service load.

Figure 13.2 also compares the predicted flexural strengths from the sectional and finite element analyses. The finite element analysis, assuming the loss of 11.25 tendons, agrees reasonably well with the sectional analysis prediction at this same degree of corrosion.
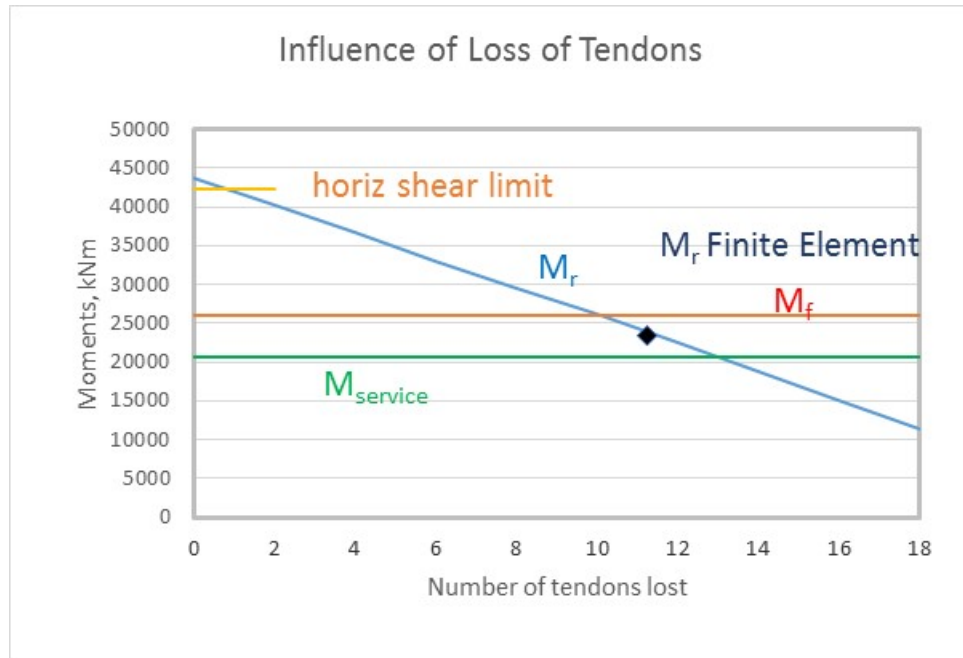
Fig. 13.2: Comparison of predicted factored flexural resistance using a sectional analysis and using the non-linear finite element model.

For all of the 2D nonlinear analyses, flexural failure near midspan was the controlling failure mode, even for the shear loading cases investigated.

It is concluded that unacceptable cracking at midspan could occur, under the CSA S6-06 service load level, when 6 to 8 tendons are lost due to corrosion. The factored flexural resistance, determined in accordance with CSA S6-06, would be insufficient when 10 tendons are lost at midspan due to corrosion.

13.4 Comparison of Effectiveness of Different Strengthening Measures

Figure 13.3 compares the level of live loading required to cause cracking in the midspan region of girder P7 for different scenarios and assuming 11.25 tendons corroded at midspan and 40% corrosion of the tendons and stirrups outside of the midspan region.

The original design is predicted to be able to carry between 2.5 and 3.1 times the service live load before cracking would occur. The girder with corrosion and no strengthening measures is predicted to carry between 0.3 and 0.5 times the service live load before cracking would occur. The level of PTE investigated on girder P7 gives an unacceptably low level of live load, between 0.4 and 0.6 times the full service live load to cause cracking. The prestressing level investigated for QP1 resulted in no cracking predicted at service load level. Strengthening using the level of

48

post-tensioning assumed in the analysis for QP2 results in no predicted cracking at service load assuming short-term properties and some predicted cracking for the case of long-term properties.
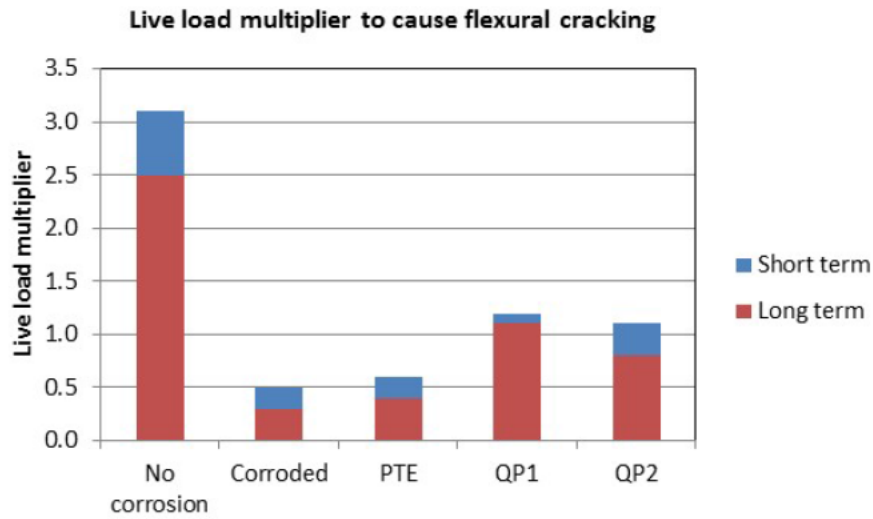

Fig. 13.3: Live load multiplier to cause flexural cracking.

Figure 13.4 shows the predicted maximum crack widths at service load level in the bottom of the flange, in the flange taper and in the web of girder P7. For the original design no cracks are predicted to occur under service loading. The predicted cracking for the corroded girder P7 before strengthening and for the case of PTE that was added to P7, at service is unacceptable. The strengthening with QP1, for the high level of post-tensioning assumed resulted in no predicted cracking. For the case of QP2, some cracking was predicted for the long-term material properties.
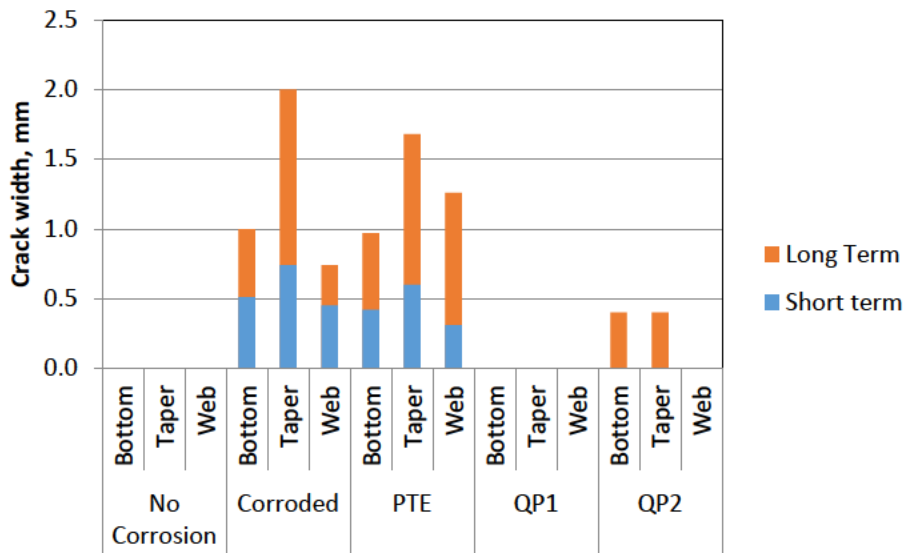

Figure 13.4: Predicted maximum crack widths at service load level in the bottom of the flange, in the flange taper and in the web of girder P7 for different scenarios.

49

Figure 13.5 shows the predicted demand-to-capacity ratios, D/C, for the different scenarios. The D/C ratios vary from 0.68 for the original design to an unacceptable value of 1.07 for the case of P7 with corroded tendons and corroded stirrups without strengthening. The case with the addition of PTE to the corroded girder is also deficient with a D/C ratio of 1.03. The levels of post-tensioning for the QP1 and QP2 strengthening resulted in acceptable D/C ratios (that is, less than 1.0).
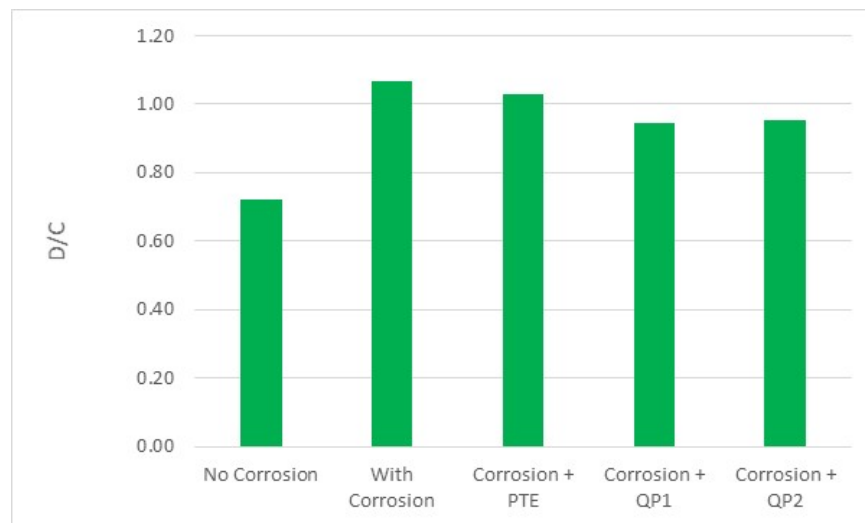

Fig. 13.5: Predicted demand-to-capacity ratios, D/C, for the different scenarios.

It is noted that the QP1 and QP2 strengthening measures are typically applied to the edge girders after PTE has been applied. This combination improves the predicted responses.

It is concluded that the original design was acceptable in terms of serviceability and strength and provided a margin of safety.

The degree of corrosion experienced in girder P7 in span 28W-29W resulted in severe cracking at service load and an inadequate flexural resistance.

The addition of the level of PTE studied, without additional strengthening measures was found to be inadequate for the degree of corrosion assumed in the analysis.

The levels of post-tensioning assumed in the analysis of QP1 and QP2 resulted in improved behaviour with QP1 resulting in acceptable performance at the service and ultimate levels. The addition of PTE to the QP2 strengthening would likely also lead to no cracking at service load levels.

14.   References

AECOM, 2011, « Pont Champlain, Sections 4, 5 and 6, réfection des piles, chevêtres, poutres et joints de tablier (2012-2013) », Contrat no. 61579, dessins 125570.

ASTM, A416/A416M-10, « Standard Specification for Steel Strand, Uncoated Seven-wire for Prestressed Concrete.

ASTM, A722/A722M-12, « Specification for Uncoated High-Strength Steel Bars for Prestressing.

Bentz, E.C. (2015), http://www.ecf.utoronto.ca/~bentz/r2k.htm, Response-2000 webpage last accessed 2015/02/13.

CSA S6-06, 2006, "Canadian Highway Bridge Design Code", Canadian Standards Association, Mississauga, ON.

Les Consultants S.M. Inc., 1999, « Rapport D'Inspection Final – Réparation de huit poutres en béton précontraint », Contrat no. 92-40-8767, mars 1999.

PJCCI, 1998, « Pont Champlain, Sections 5 & 7 Réfection de 8 Poutres de Béton (1998) – Détails de Renforcement des Poutres par Post-Tension », No. Contrat 92-40-8767, No. Dessin 125101-06.

TECHNISOL INC., 2006, « Pont Champlain – Section 5 & 7 - Expertise sur le Béton des Poutres de Béton Précontraint », La Société Les Ponts Jacques Cartier & Champlain Inc., Contrat 60862, Avril 2006.

Vecchio, F.J. (2015), http://www.civ.utoronto.ca/vector, VecTor2 webpage, last accessed 2015/02/13.

Warycha, L. and Skotecky, C., "Construction of Piers and Superstructure - Section 5 and 7A of Champlain Bridge – I Explanatory Note – Calculation and References", Document 0277.